Post-mitotic accumulation of histone variant H3.3 in new cortical neurons establishes neuronal transcriptome, identity, and connectivity

Owen H. Funk[1,2], Yaman Qalieh[1,2], Daniel Z. Doyle[1,2,3], Mandy M. Lam[1,2], Kenneth Y. Kwan[1,2,3]

1. Michigan Neuroscience Institute (MNI), University of Michigan, Ann Arbor, MI 48109, USA
2. Department of Human Genetics, University of Michigan, Ann Arbor, MI 48109, USA
3. Neuroscience Graduate Program, University of Michigan, Ann Arbor, MI 48109, USA

*Correspondence should be addressed to K.Y.K. (kykwan@umich.edu)

Abstract

Histone variants, which can be expressed outside of S-phase and deposited DNA synthesis-independently, provide replacement histones in terminally post-mitotic cells, including neurons. Histone variants can also serve active roles in gene regulation by modulating chromatin states or enabling nucleosome turnover at regulatory regions. Here, we find that newborn cortical excitatory neurons substantially accumulate the histone H3 variant H3.3 immediately post-mitosis. Co-deletion of H3.3-encoding genes *H3f3a* and *H3f3b* from new neurons abrogates this accumulation, and causes widespread disruptions in the developmental establishment of the neuronal transcriptome. These broad transcriptomic changes coincide with neuronal maturation phenotypes in acquisition of distinct neuronal identities and formation of axon tracts. Stage-dependent deletion of *H3f3a* and *H3f3b* from (1) cycling neural progenitor cells, (2) neurons immediately after terminal mitosis, or (3) several days later, reveals the first post-mitotic days as a critical window for *de novo* H3.3. After H3.3 accumulation within this developmental window, co-deletion of *H3f3a* and *H3f3b* from neurons causes progressive H3.3 depletion over several months without widespread transcriptional disruptions. Our study thus uncovers a key role for H3.3 in establishing neuronal transcriptome, identity, and connectivity immediately post-mitosis that is distinct from its role in maintaining total histone H3 levels over the neuronal lifespan.

Significance

DNA is tightly packaged around histones into chromatin, which compacts the genome, but also restricts access to DNA. All transactions on DNA, notably gene transcription, require chromatin reorganization that is precisely regulated, including via the use of variant forms of histones. Here, we find that during a critical developmental window for establishing post-mitotic neuronal identity, newly generated cortical excitatory neurons substantially accumulate the histone H3 variant H3.3 immediately after terminal mitosis. Conditional deletion of H3.3-encoding genes from new neurons abrogates this accumulation, and disrupts neuronal gene expression, subtype identity, and axon projections. Thus, H3.3 plays important roles in establishing neuronal transcriptome, identity, and connectivity during post-mitotic development. These functions are distinct from long-term maintenance of histone levels in mature neurons.

Introduction

Nuclear DNA is packaged into chromatin around histones, which compact the genome, but also constrain biological processes on DNA. Chromatin regulation, for example via chromatin remodeling, histone post-translational modifications (PTMs), or histone variants, contributes to all transactions on DNA, including transcription and DNA damage repair (1-8). In dividing cells, canonical histones are highly expressed in S-phase and are assembled into nucleosomes in a DNA replication-coupled manner (2, 5, 9-11), thereby meeting the demand for new histones to package newly synthesized DNA. Histone variants, however, are expressed throughout the cell cycle and can be incorporated DNA synthesis-independently (2, 5, 11-14). These variants therefore replenish histones that are turned over in post-mitotic cells (12, 15-17), including terminally post-mitotic

neurons. In addition to replacing canonical histones, histone variants can also mark specific genomic regions, modulate chromatin states, influence interactions with chromatin regulators, and regulate nucleosome turnover, thereby serving more active roles in mediating specific chromatin functions, most notably gene regulation (3, 5, 18-22).

Histone H3, one of four core histone proteins, is characterized by a protruding N-terminal tail particularly amenable to PTMs that modulate chromatin function, including H3K27me3 and H3K4me3. Canonical H3.1 and H3.2 are encoded by dozens of genes that are clustered, transcribed in S-phase, lack introns, and terminate in a stem-loop structure without polyadenylation (2, 5, 11, 12, 23-27). The deposition of canonical H3 is DNA synthesis-dependent, occurring exclusively in S-phase. The H3 variant H3.3, in contrast, is encoded by *H3f3a* and *H3f3b*, which undergo splicing, terminate by polyadenylation, and are expressed throughout the cell cycle, including in S-phase (2, 5, 11, 12, 23-27). Unlike canonical H3, variant H3.3 is incorporated replication-independently into the genome, preferentially at enhancers, promoters, and gene bodies (18, 20, 28-33), a pattern that suggests H3.3 roles in gene regulation. Functional studies have shown H3.3 involvement in diverse processes, including myogenesis, neural crest cell differentiation, gametogenesis, genome maintenance, and zygotic genome activation (34-39). In the brain, silencing of H3.3 genes by RNA interference leads to deficits in neuronal layer distribution, activity- and environmental enrichment-induced gene expression, and memory (21, 40).

Here, we use conditional genetics to stage-dependently manipulate H3.3-encoding genes *H3f3a* and *H3f3b* during cerebral cortex development. We find that despite near ubiquitous mRNA expression of *H3f3a* and *H3f3b* in the developing cortex, including in cycling cortical neural progenitor cells (NPCs) and terminally post-mitotic excitatory neurons, H3.3 protein levels are not uniform. Whereas NPCs are characterized by low H3.3 levels, newborn cortical neurons undergo substantial *de novo* accumulation of H3.3 immediately post-mitosis. Co-deletion of *H3f3a* and *H3f3b* from newly post-mitotic neurons abrogates this increase and causes widespread disruptions in the developmental establishment of the neuronal transcriptome. These transcriptomic changes coincide with neuronal maturation phenotypes, including in acquisition of distinct neuronal identities and formation of cortical axon tracts. By stage-dependent deletion of H3.3-encoding genes from: 1) cycling NPCs; 2) neurons immediately after terminal mitosis; or 3) neurons several days after final mitosis, we identify the first few post-mitotic days as a critical window for *de novo* H3.3 in cortical neurons. After initial H3.3 accumulation in this developmental window, co-deletion of *H3f3a* and *H3f3b* causes progressive loss of H3.3 over several months without widespread disruptions to the transcriptome. Thus, our study uncovers an active role for H3.3 in establishing the transcriptional landscape, molecular identity, and axon connectivity in developing neurons immediately post-mitosis that is distinct from its role in maintaining histone H3 levels over the neuronal lifespan.

Results

H3f3a and *H3f3b* were widely expressed in developing cortex

H3.3 protein is encoded by *H3f3a* and *H3f3b*, which are broadly expressed in many tissues (24, 41). To determine the expression of H3.3 genes at the level of single cells, we used single nuclei (sn)RNA-seq to analyze wildtype embryonic day (E)14.5 cortex on the 10x Chromium platform. We assayed 9,300 cells that met stringent quality control for snRNA-seq, with a median of 2,642 genes detected per cell. Clustering by Seurat (42) revealed 18 groups that encompassed the full complement of known cell types in embryonic cortex (**Fig. 1A**). Our analysis revealed high *H3f3a* and *H3f3b* expression levels in all types of NPCs, including radial glial cells (RGCs) and intermediate progenitor cells (IPCs), as well as post-mitotic neurons at various stages of maturation (**Fig. 1A**). Each of the 18 cell types expressed *H3f3a* and *H3f3b* (**Fig. 1A**). At the level of single cells, *H3f3a* was detected in 9,113/9,300 cells (98.0%) and *H3f3b* was detected in 9,132/9,300 cells (98.2%). Consistent with bulk and scRNA-seq of the developing human cortex (43, 44), our data indicated that *H3f3a* and *H3f3b* were widely, likely

ubiquitously, expressed in the developing cortex. This is further consistent with previous reports that *H3f3a* and *H3f3b* are expressed ubiquitously and throughout the cell cycle (24, 45).

New neurons substantially accumulated H3.3 post-mitosis

To assess H3.3 protein levels in individual cells, we used H3.3-specific immunostaining on embryonic wildtype cortex. At E14.5, NPCs in ventricular zone (VZ) and subventricular zone (SVZ) were characterized by low levels of H3.3 proteins (**Fig. 1B** and **Supp. Fig. 1A**). In contrast, post-mitotic neurons in cortical plate (CP) were characterized by high H3.3 levels, suggesting that H3.3 protein levels increased post-mitotically. At E16.5, H3.3 levels in NPCs remained low. In post-mitotic neurons, however, H3.3 levels were not only comparatively higher, but began to show a layer-dependent gradient; higher in deeper portions of the cortex and lower in more superficial parts (**Fig. 1B** and **Supp. Fig. 1B**). In the developing cortex, excitatory neurons are generated sequentially (subplate neurons → deep layer neurons → upper layer neurons) and settle in the cortex in an inside first, outside last manner (46-48). At E16.5, the earliest born subplate (SP) and lower layer (L5/L6) neurons were characterized by the highest levels of H3.3, the next-born neurons of the deep CP showed comparatively lower levels of H3.3, and the most recently-born upper CP neurons had the lowest levels of H3.3 (**Fig. 1B** and **Supp. Fig. 1B**). This gradient suggested that H3.3 accumulation occurred progressively over several days following exit from the cell cycle. In contrast to H3.3 specific staining, pan-H3 staining was uniform throughout the cortex, without the gradient seen in H3.3 (**Fig. 1B**). The high level of pan-H3 staining in NPCs, in which H3.3 staining was low, is consistent with canonical H3 (H3.1 and H3.2) deposition in cycling cells (49, 50). At P0, the latest born cortical neurons, located at the upper edge of L2/3, were characterized by low H3.3 staining, but similar pan-H3 staining compared to the earlier-born deep layer neurons (**Fig. 1B**). Importantly, by P7, the layer gradient in H3.3 staining had disappeared; both deep and upper layer neurons were characterized by high levels of H3.3 (**Supp. Fig. 1C**). This finding suggests that the layer difference in H3.3 levels at E16.5 and P0 (**Fig. 1B**) reflected the age of neurons since final mitosis, and that by P7, late-born upper layer neurons have had sufficient time to reach H3.3 levels similar to earlier-born deep layer neurons. To directly quantify H3.3 levels from the time of neuronal birth, we labeled wildtype embryos by a pulse of thymidine analog 5-ethynyl-2´-deoxyuridine (EdU) at E13.5, and tracked labeled cells 2h, 24h, 3 days, 5 days, or 6 days later. We found that in S-phase cells labeled by a 2h pulse of EdU, H3.3 was present only at low levels (**Fig. 1C**). Over the next 6 days following neuronal birth, H3.3 levels progressively increased in EdU-labeled neurons (**Fig. 1C** and **D**). Together, our data indicated that although *H3f3a* and *H3f3b* were expressed throughout the cell cycle, H3.3 histone accumulation in neurons significantly increased post-mitotically over several days following the final mitosis (**Fig. 1E**).

Conditional co-deletion of H3.3 genes *H3f3a* and *H3f3b* from post-mitotic neurons or cycling NPCs

The H3.3 genes *H3f3a* and *H3f3b* encode the same H3.3 protein (9, 10, 51). Constitutive co-deletion of *H3f3a* and *H3f3b* leads to peri-implantation lethality by E6.5 in mice (39) and zygotic knockdown of both genes leads to a significant decrease in successful blastulation (35). To study the roles of H3.3 in cortical development, we leveraged conditional alleles of *H3f3a* and *H3f3b* (52). These alleles were each designed with a reporter; Cre recombination of the *H3f3a* floxed allele deletes *H3f3a* and turns on Venus reporter expression, whereas Cre recombination of the *H3f3b* floxed allele deletes *H3f3b* and turns on Cerulean reporter expression (**Supp. Fig. 1D**) (52). To distinguish potential H3.3 functions in post-mitotic neurons versus cycling NPCs prior to final neuronogenic mitosis, we used two complementary Cre lines for conditional deletion. First, to assess the role of post-mitotic H3.3 deposition, we used *Neurod6*^{Cre} (*Nex*^{Cre}), which mediates recombination in new-born excitatory neurons immediately after terminal mitosis, without affecting NPCs (53). Second, to assess the role of the comparatively lower levels of H3.3 in NPCs, we used *Emx1*^{Cre}, which mediates recombination in cortical NPCs starting at E10.5 (54), prior to the onset of neuronogenesis. We confirmed the published patterns of CRE expression in these lines at E14.5 (**Fig. 1F**), and the cell-type specificity and efficiency of Cre-mediated H3.3 floxed allele recombination by reporter expression (**Supp. Fig. 1E**).

The resulting double H3.3 gene conditional knockouts, *Neurod6*^{Cre};*H3f3a*$^{f/f}$;*H3f3b*$^{f/f}$ (dKO-N) and *Emx1*^{Cre};*H3f3a*$^{f/f}$;*H3f3b*$^{f/f}$ (dKO-E) were born alive. Both dKO-N and dKO-E, however, were characterized by complete early postnatal lethality within several hours of live birth accompanied by absence of milk spot, which suggested an inability to suckle. In contrast, mice with one or more wildtype allele of H3.3 gene, either *H3f3a* or *H3f3b*, were not affected by early lethality; they lived into adulthood and were fertile as adults.

Post-mitotic deletion of *H3f3a* and *H3f3b* abrogated H3.3 accumulation in neurons

To assess H3.3 accumulation following conditional deletion of *H3f3a* and *H3f3b*, we used H3.3 specific immunostaining. We found that neuronal (dKO-N) or NPC (dKO-E) deletion of *H3f3a* and *H3f3b* led to an extensive loss of H3.3 from P0 cortex (**Fig. 1G**), but not from subcortical brain structures. Pan-H3 levels, in contrast, were unaffected (**Fig. 1G**). Thus, co-deletion of *H3f3a* and *H3f3b*, in dKO-N or dKO-E, abrogated H3.3 synthesis and led to loss of H3.3, but not pan-H3, by P0. Notably, co-deletion of H3.3 genes from post-mitotic neurons in dKO-N resulted in H3.3 loss highly similar to dKO-E (**Fig. 1G**), an observation that was supported by H3.3 immunoblotting (**Supp. Fig. 1F**). This similarity indicated that *H3f3a* and *H3f3b* gene expression from NPCs, which was preserved in dKO-N, was insufficient for H3.3 accumulation in neurons; post-mitotic expression of H3.3 genes was required. This finding is consistent with our observation that neurons underwent significant H3.3 accumulation post-mitosis (**Fig. 1B**) and supported that *de novo*, neuronal H3.3 expression was necessary for this post-mitotic increase.

Deletion of H3.3 genes was not cell autonomously lethal

To assess the phenotypic consequences of conditional *H3f3a*/*H3f3b* co-deletion, we analyzed the mutants at P0. Whole mount P0 brains showed no significant loss of cortical tissue in dKO-N or dKO-E, whereas quantification of cortical thickness revealed a minor reduction (**Supp. Fig. 1G-I**). Importantly, despite loss of H3.3 from cortical neurons, both dKO-N and dKO-E were characterized by an abundance of reporter-expressing cells (**Supp. Fig. 1J**), indicating that loss of H3.3 did not cause widespread cell loss, unlike some models of chromatin dysregulation (55-57). This finding was consistent with immunostaining for cleaved caspase 3 (CC3), a marker of apoptosis, and phospho-(p)KAP1 (TRIM28), a marker of DNA double-strand breaks (**Supp. Fig. 1K**). Together, these data showed that loss of H3.3 from cortical neurons in dKO-N and dKO-E did not cause extensive cell lethality or DNA damage.

Defects in developmental acquisition of neuronal transcriptome following *H3f3a* and *H3f3b* co-deletion

H3.3 can contribute to transcriptional regulation by selective incorporation into regulatory regions, PTMs, interactions with chromatin regulators, or nucleosome turnover (13, 18-22, 28, 30, 58, 59). To assess the potential transcriptional roles of post-mitotic H3.3 accumulation in neurons, we studied the consequences of post-mitotic *H3f3a* and *H3f3b* co-deletion by transcriptomic analyses of dKO-N and littermate control cortices at P0. We generated sequencing libraries for unique molecular identifier (UMI) RNA-Seq by Click-seq (60). For UMI RNA-seq, we barcoded each individual cDNA molecule by addition of a UMI tag such that PCR-amplified reads can be de-duplicated after sequencing, which enabled highly quantitative measurements of expression levels (61) (**Supp. Fig. 2A**). Differential gene expression was analyzed using edgeR (62). This revealed significant changes meeting a stringent FDR of < 0.01 in 948 genes in cKO-N compared to control (**Fig. 2A**). Of these differentially regulated genes (DEGs), 579 were significantly downregulated ($\log_2 FC < 0$) and 369 were significantly upregulated ($\log_2 FC > 0$).

The early post-mitotic accumulation of H3.3 coincided with an important period of molecular identity acquisition and refinement for new neurons. To determine whether co-deletion of H3.3 genes affected the

developmental establishment of the transcriptional landscape, we intersected genes that were significantly downregulated (579), upregulated (369), or unchanged (3128, FDR > 0.9, $-0.1 < \log_2FC < 0.1$, $\log_2CPM > 1$) in dKO-N with wildtype embryonic forebrain gene expression data from ENCODE at multiple developmental timepoints (E10.5 to P0) (63). This revealed in downregulated DEGs an overrepresentation of genes with a strongly positive developmental trajectory (i.e., a progressive increase in expression across normal forebrain development) (**Fig. 2B**). This enrichment, which was absent from genes that were unchanged in dKO-N, suggested that following neuronal *H3f3a*/*H3f3b* co-deletion, some genes that normally increase in expression during development failed to do so. We confirmed this finding by using logistic regression on the ENCODE data to identify all genes that normally increase over the course of embryonic forebrain development (i.e., with a significantly positive trajectory; slope > 2, pval < 0.01) (**Fig. 2C**). As a group, these genes were significantly downregulated in dKO-N, consistent with a role for H3.3 in upregulating neuronal genes to establish the transcriptome post-mitosis. Genes that normally decrease over development (i.e., with a significantly negative trajectory; slope < -2, pval < 0.01) were moderately increased in dKO-N, whereas genes that maintained expression levels across development were broadly unaffected (**Fig. 2C**). Together, these data indicated that transcriptomic defects following neuronal *H3f3a*/*H3f3b* deletion included specific deficits in the developmental acquisition of the neuronal transcriptome.

H3.3 can influence gene expression via regulatory PTMs. To determine whether the differentially expressed genes following neuronal *H3f3a*/*H3f3b* deletion were preferentially marked by certain histone H3 PTMs, we used ENCODE ChIP-seq data from wildtype E10.5 to P0 forebrain for intersectional analyses (63). This revealed that downregulated DEGs in dKO-N are characterized by dynamic PTM shifts over normal forebrain development. At earlier timepoints (e.g., E10.5) they are associated with both H3K27me3 and H3K4me3 (**Fig. 2D**), which together mark a bivalent chromatin state that can be resolved into active transcription or repressive silencing (64-66). As development progressed, H3K4me3 enrichment is maintained at these genes, but H3K27me3 enrichment is progressively lost, indicating that these genes are normally resolved into a transcriptionally active chromatin state over embryonic development (**Fig. 2D**). These included dKO-N differentially expressed genes *Nwd2*, *Zfp385b*, and the neuronal differentiation marker *Rbfox3* (*NeuN*) (**Supp. Fig. 2B**). Together, these data suggest that in the absence of *de novo* H3.3 in neurons, some bivalent genes that normally resolve into active transcription over the course of cortical development did not developmentally upregulate their transcription, thus resulting in reduced expression levels in P0 dKO-N compared to control.

To determine whether the comparatively lower levels of H3.3 within NPCs (**Fig. 2B**) contribute to gene regulation, we analyzed the P0 cortical transcriptome of dKO-E, in which *H3f3a*/*H3f3b* were co-deleted from cycling NPCs. This revealed in dKO-E 1934 DEGs, of which 964 were significantly downregulated and 970 were significantly upregulated compared to control (**Fig. 2E**). Although the number of genes meeting FDR < 0.01 was higher in dKO-E compared to dKO-N, differential gene expression analysis (**Fig. 2F**) and analysis of hypergeometric distributions (**Fig. 2G**) revealed significantly overlapping transcriptomic changes between dKO-E and dKO-N. In support of this, the genes that were differentially expressed in dKO-E were remarkably consistent in expression change directionality in dKO-N (**Fig. 2H**). Similarly, the genes that were differentially expressed in dKO-N were also comparably changed in dKO-E. Thus, these analyses revealed that *H3f3a*/*H3f3b* deletion from NPCs prior to final mitosis (dKO-E) led to significantly overlapping gene expression changes compared to *H3f3a*/*H3f3b* deletion from neurons post-mitosis (dKO-N). Together, our transcriptomic results support an important post-mitotic role for H3.3 in the developmental establishment the neuronal transcriptome.

Defects in deep-layer neuron identities following *H3f3a* and *H3f3b* co-deletion

The cerebral cortex is specified into six cytoarchitectonically distinct laminae, each with a characteristic composition of molecularly defined neurons (47, 67). To assess whether the transcriptional deficits following *H3f3a* and *H3f3b* co-deletion accompanied altered development of cortical laminae, we first used

immunostaining for RBFOX3 (NEUN), a neuronal differentiation marker (68). In P0 control, RBFOX3 immunostaining was present in all cortical layers but more intensely labeled L5 and subplate (SP) neurons (**Fig. 3A**). In both dKO-N and dKO-E, RBFOX3 immunostaining was reduced in all cortical layers, and the intense labeling of L5 and SP neurons was lost (**Fig. 3A**). We next used layer markers to assess layer-dependent molecular identities. In control, BCL11B (CTIP2) showed intense staining in L5 neurons and moderate staining in L6 neurons in a highly stereotyped pattern (69, 70) (**Fig 3B**). In both dKO-N and dKO-E, however, this stereotypic distinction was lost; although BCL11B staining was correctly present in deep layers, a clear differential staining between L5 and L6 was absent. This change was accompanied by additional disruptions of deep-layer marker expression. In control P0 cortex, intense BHLHE22 staining was present in L5 neurons, whereas TLE4 staining was restricted to L6 neurons (**Fig. 3C**). In both dKO-N and dKO-E, the L5 staining of BHLHE22 was lost, whereas TLE4 staining extended beyond L6 and was aberrantly present in L5 (**Fig. 3C**). Thus, the identities of deep-layer cortical neurons were perturbed following *H3f3a*/*H3f3b* co-deletion. Notably, these laminar phenotypes were indistinguishable between dKO-E and dKO-N, suggesting that the requirement for H3.3 in layer-dependent gene expression is post-mitotic.

Neuronal identity is defined by combinatorial gene expression. We therefore assessed the molecular specification of neurons using BCL11B and TLE4 co-immunostaining (**Supp. Fig. 3A**), and BCL11B and TBR1 co-immunostaining (**Supp. Fig. 3B**). In P0 control cortex, L6 neurons were intensely labeled by TLE4 and TBR1 and weakly labeled by BCL11B, whereas L5 neurons were characterized by intense BCL11B labeling and an absence of TLE4 and TBR1, similar to previous reports (69, 71, 72). In dKO-N, however, L5 and L6 neurons were strongly co-labeled by BCL11B and TLE4 (**Supp. Fig. 3A**) and BCL11B and TBR1 (**Supp. Fig. 3B**). Thus, in the absence of *de novo* neuronal H3.3, deep-layer neurons did not acquire fully distinct L5 versus L6 identities.

The molecular identities of deep-layer neurons are not solely established during neurogenesis; they undergo progressive post-mitotic refinement (70). For example, newly post-migratory L6 neurons transiently co-express both L5 and L6 markers, but subsequently downregulate L5 markers at late fetal ages to establish their L6-specific identity (70). To determine whether neuronal H3.3 contributes to this post-mitotic refinement, we used co-immunostainings to assess the divergence of L5 versus L6 identities over development in dKO-N. In control E15.5 cortex, L6 neurons abundantly co-expressed BCL11B and TBR1, and BCL11B and ZFPM2 (FOG2) (**Fig. 3D**). In E17.5 control, L6 neurons have begun to downregulate BCL11B. By P0, TBR1- or ZFPM2-labeled L6 neurons largely did not express high levels of BCL11B (**Fig. 3D**), consistent with the developmental downregulation of L5 expression in the acquisition of L6 identity (70). In dKO-N E15.5 cortex, L5 and L6 markers were co-expressed in a manner similar to control (**Fig. 3E**). At E17.5 and P0, however, deep-layer neurons aberrantly maintained abundant L5 and L6 marker co-expression in dKO-N; BCL11B expression had not been downregulated from TBR1- or ZFPM2-labeled L6 neurons. Therefore, in the absence of neuronal H3.3, deep-layer neurons aberrantly maintained mixed L5/L6 molecular identity postnatally. To determine whether aberrant marker co-expression was also present in upper-layer neurons in dKO-N, we used BCL11B and SATB2 co-immunostaining (**Supp. Fig. 3C**). BCL11B and SATB2 are mutually repressive markers that respectively label corticofugal and intracortical projection neurons (73, 74). In P0 control, BCL11B and SATB2 labeled largely distinct neurons in the deep layers, and SATB2, but not BCL11B, was present in the upper layers, consistent with previous studies (67, 75). In dKO-N, upper-layer neurons correctly expressed SATB2, and did not misexpress BCL11B (**Supp. Fig. 3C**). Together, these data suggest that although deep-layer neuronal identities became molecularly mixed, an upper- versus deep-layer molecular distinction was present following neuronal deletion of *H3f3a*/*H3f3b* in dKO-N.

Defects in cortical axonal projections following *H3f3a* and *H3f3b* co-deletion

The pathfinding of cortical axons is dependent on correct specification of laminar identities (47, 67), as well as axon guidance mediated by subplate neurons (70, 76, 77). To assess whether axonal phenotypes

accompanied the transcriptomic and layer organization changes following *H3f3a*/*H3f3b* co-deletion, we analyzed cortical axon tracts in P0 cortex (**Fig. 4A**). In control cortex, immunostaining of L1CAM, an axon marker, revealed axons traversing white matter (WM) below cortical plate (CP) (**Fig. 4B**). L1CAM also labeled the trajectory of the corpus callosum (CC), which normally connects the left and right cortical hemispheres (**Fig. 4B**). *H3f3a* and *H3f3b* co-deletion from neurons (dKO-N) or NPCs (dKO-E) led to a marked loss of white matter thickness, and complete agenesis of corpus callosum (**Fig. 4B**). Next, we leveraged the Cre-dependent fluorescent reporters expressed from the *H3f3a* and *H3f3b* floxed loci (**Supp. Fig. 1D**) to analyze axon tracts. In both dKO-N and dKO-E, the anterior commissure (AC), which normally connects lateral cortical regions, failed to cross the midline and was misrouted towards the hypothalamus (**Fig. 4C**). In addition to intracortical tracts, corticofugal tracts were also disrupted. In both dKO-N and dKO-E, corticofugal axons projected into the caudate putamen (CP) and innervated the internal capsule (IC) (**Fig. 4D**), where corticofugal axons normally coalesce before diverging towards their respective subcortical targets. Beyond the internal capsule, however, corticofugal axons showed deficits in reaching their subcortical targets in both dKO-N and dKO-E. Analysis of the corticothalamic tract, which was abundantly visible in control, revealed a near complete absence of cortical axons reaching the dorsal thalamus (**Fig. 4D**). Similarly, analysis of the corticospinal tract (CST) also revealed an absence of axons that reached the level of the pons or beyond (**Fig. 4E**). Thus, efferent axons were able to successfully extend out of the cortex in the absence of H3.3, but were largely unable to reach their final targets. We further analyzed the axons of hippocampal pyramidal neurons (**Supp. Fig. 4A**). In both dKO-N and dKO-E, hippocampal axons projected into the fimbria, but failed to innervate the fornix. These deficits accompanied alterations in hippocampal organization (**Supp. Fig. 4B** and **D**). Together, these data revealed a requirement for H3.3 in the formation of both intracortical and corticofugal tracts, especially in enabling axons to reach their final targets in the contralateral hemisphere or in subcerebral brain structures. Importantly, these axonal defects were phenotypically indistinguishable between dKO-N and dKO-E, indicating that the requirement for *de novo* H3.3 in axon tract development is largely post-mitotic.

H3f3a and *H3f3b* co-deletion after initial H3.3 accumulation

The substantial *de novo* H3.3 accumulation that we found in new cortical neurons occurred in the first few days after terminal mitosis (**Fig. 1**). In the absence of this accumulation following *H3f3a*/*H3f3b* co-deletion immediately post-mitosis (dKO-N), cortical neurons were unable to acquire the neuronal transcriptome or undergo developmental maturation, suggesting an active role for *de novo* H3.3 in the first few postmitotic days. H3.3 can be deposited DNA synthesis-independently (2, 24). In terminally post-mitotic cells such as neurons, H3.3 is thought to be the primary source of new histone H3, thus serving important long-term functions in maintaining overall H3 levels (15). H3.3 has also been shown to be involved in neuronal senescence, plasticity, and activity-dependent gene expression (21). To assess the longer term roles of H3.3 in cortical neurons, we generated an additional *H3f3a*/*H3f3b* co-deletion model using Tg(*Rbp4-Cre*) (78, 79). Tg(*Rbp4-Cre*) mediates recombination from L5 neurons starting at ~E18.5 (**Fig. 5A**), after substantial *de novo* H3.3 accumulation had occurred in the first few post-mitotic days. Importantly, Tg(*Rbp4-Cre*)*;H3f3a*$^{f/f}$;*H3f3b*$^{f/f}$ (dKO-R), unlike dKO-N, was not affected by peri-natal lethality. Thus, the use of dKO-R (**Fig. 5B**) enabled us to: 1) assess the requirement for *de novo* H3.3 after the initial post-mitotic accumulation; and 2) determine the long-term turnover dynamics of H3.3 in post-mitotic neurons.

First, we sought to determine potential phenotypic differences between *H3f3a*/*H3f3b* co-deletion immediately post-mitosis (dKO-N; prior to initial H3.3 accumulation) versus ~5 days post-mitosis (dKO-R; after initial H3.3 accumulation). For direct comparison, we focused our analysis on L5 neurons, which were affected by both Tg(*Rbp4-Cre*) and *Neurod6-Cre* deletion. In dKO-N, we found robust axonal phenotypes, including a striking absence of corticospinal axons reaching the level of the pons (**Fig. 4D**). Corticospinal tract axons originate from L5 neurons, which express Tg(*Rbp4-Cre*) (78, 79). To assess corticospinal axon development in dKO-R, we used a Cre-dependent tdTomato transgene (*ROSA*$^{CAG\text{-}tdTomato}$) to label corticospinal axons originating

from L5 neurons. In P7 dKO-R, corticospinal tract (CST) axons abundantly innervated the pyramids at the level of the medulla in a manner that was indistinguishable from control (**Fig. 5C**). Furthermore, in dKO-N, we found alterations in layer-dependent neuronal identities; BCL11B staining did not differentiate L5 versus L6 neurons (**Fig. 3B**) and BHLHE22 labeling was lost from L5 neurons (**Fig. 3C**). In P7 dKO-R, however, BCL11B staining differentiated L5 and L6 neurons, and BHLHE22 intensely labeled L5 neurons, each in a manner similar to control (**Fig. 5D**). These data therefore showed that after initial H3.3 accumulation, *H3f3a*/*H3f3b* deletion in dKO-R did not disrupt the molecular identity or axon projection of L5 neurons, as *H3f3a*/*H3f3b* deletion prior to initial H3.3 accumulation did in dKO-N.

Progressive depletion of H3.3 from post-mitotic neurons

Unlike dKO-N mice, dKO-R mice survived into adulthood without premature lethality, enabling us to examine the long-term dynamics of H3.3 in post-mitotic neurons. In dKO-R, Tg(*Rbp4-Cre*) mediated *H3f3a*/*H3f3b* co-deletion after the initial accumulation of H3.3 post-mitosis. Consistent with substantial H3.3 accumulation in the first few post-mitotic days (**Fig. 1B**), our analysis of dKO-R at P0 revealed no immediate change in H3.3 levels within Tg(*Rbp4-Cre*)-expressing L5 neurons labeled by $ROSA^{CAG\text{-}tdTomato}$ (**Fig. 5E** and **F**). This contrasted dKO-N, in which *H3f3a*/*H3f3b* co-deletion from newly post-mitotic neurons led to a marked loss of H3.3 by P0 (**Fig. 1G**). To determine how H3.3 levels in dKO-R changed over time in the absence of *de novo* H3.3, we comprehensively analyzed H3.3 in L5 neurons from P0 to 6 months of age. This revealed in dKO-R a slow, progressive loss of H3.3 from L5 neurons over several months (**Fig. 5E** and **F**). These data suggested that in cortical neurons, after initial accumulation of H3.3 in the first days post-mitosis, H3.3 was turned over much more slowly, over weeks and months. In addition, the abundance of H3.3-negative neurons in dKO-R at 6 months of age indicated that H3.3 was not required for long-term survival of neurons. Consistent with this, our analysis of DNA double strand breaks by pKAP1 marker staining revealed no increase in DNA damage in dKO-R at 6 months compared to control (**Supp. Fig. 5A**).

H3.3 has been proposed to be an important source of H3 protein throughout the lifespan of post-mitotic neurons (17, 21). To assess total H3 levels in dKO-R, we used pan-H3 immunostaining at 6 months, an age at which we observed a 78.7% reduction in H3.3 levels in L5 neurons. Surprisingly, despite the marked loss of H3.3, the levels of pan-H3 were not observably different between dKO-R and control (**Fig. 5G**). The presence of histone H3 was confirmed by immunostaining for H3 that carried post-translational modifications H3K4me3 or H3K27me3 (**Fig. 5G**). These data also suggested that H3 modifications were not eliminated by the lack of *de novo* H3.3 over 6 months. Together, our data supported that following loss of *de novo* H3.3 synthesis, H3.3 levels progressively decreased over several months. Despite loss of H3.3, total H3 levels were maintained up to six months postnatally, suggesting that H3.3 may not be the sole source of H3 proteins in terminally post-mitotic neurons.

Maintenance of neuronal transcriptome following progressive H3.3 depletion

Our results revealed a substantial accumulation of H3.3 in the first days post-mitosis (**Fig. 1**) that was required for establishing neuronal transcriptome and identity (**Fig. 2** and **Fig. 3**). The timescale of this initial accumulation contrasted long-term H3.3 turnover, which we found to occur over weeks and months in neurons (**Fig. 5**). To assess the consequences of H3.3 depletion on the maintenance of neuronal transcription, we used snRNA-seq to analyze control and dKO-R cortex at 5 weeks, after significant loss of H3.3. Clustering by Seurat (42) revealed 34 groups that encompassed the full complement of known cell types in postnatal cortex (**Fig. 6A**). Remarkably, the clustering of control and dKO-R cells showed the same clusters in nearly identical UMAP space (**Fig. 6A**) and substantial overlap of each individual cluster (**Fig. 6B**), including the L5 pyramidal tract (PT) neuron in which Tg(*Rbp4-Cre*) was active (78, 79). This overlap was in striking contrast to the widespread transcriptomic changes we found in dKO-N (**Fig. 2**). We further used differential expression analysis of the L5 PT cluster and

specifically assessed whether the differentially-expressed genes (DEGs) in dKO-N were similarly affected in dKO-R L5 PT. We found that each dKO-N DEGs, both up- and down-regulated, became remarkably normalized towards a $\log_2$FC of 0 (i.e., no change) (**Fig. 6C**). Together, these data suggest that although the initial accumulation of H3.3 was required to establish the expression of these genes in neurons, once established, *de novo* H3.3 was no longer required to maintain their expression. These data are further consistent with a lack of significant loss of total H3 or H3 carrying PTMs in dKO-R despite loss of H3.3, and the possibility of a non-H3.3 source of H3 that can maintain overall H3 levels in post-mitotic neurons. Our analysis did reveal 71 genes that were modestly differentially regulated in dKO-R L5 PT neurons. Interestingly, a number of these genes are associated with synapse activity, consistent with previous reports that in mature neurons, H3.3 can play a longer-term role in neural plasticity (17, 21).

DISCUSSION

De novo H3.3 in newly post-mitotic neurons

In the first post-mitotic days, cortical excitatory neurons undergo a series of molecular and cellular processes to establish their transcriptional identity and axonal connectivity. We find that during this crucial developmental period, post-mitotic neurons progressively accumulate the histone H3 variant H3.3. Prior to final mitosis, cycling NPCs are characterized by low levels of H3.3. After terminal division, neurons substantially accumulate H3.3 over the first several post-mitotic days. This accumulation requires *de novo* H3.3 in newly post-mitotic neurons. Our *in vivo* results are consistent in timing with *in vitro* data from primary neurons, which reached sustained H3.3 levels only after 9 days in culture (21). As a variant histone, H3.3 is thought to serve as the primary source of replacement H3, maintaining histone levels in terminally post-mitotic cells, including neurons. Previous studies have shown that in the adult brain and other tissues, H3.3 progressively replaces canonical H3.1 and H3.2 over several months after birth (15-17, 21). In contrast to H3 maintenance over the neuronal lifespan, the late fetal, early post-natal H3.3 accumulation we describe occurs in new neurons shortly after the final mitosis. The selective timing of this post-mitotic H3.3 accumulation is notable because *H3f3a* and *H3f3b* are expressed ubiquitously and throughout the cell cycle. Furthermore, canonical H3.1 and H3.2 are produced at high levels in S-phase to meet the demand for histones on newly synthesized DNA (25). The requirement for *de novo* H3.3 in newborn neurons, which have only recently undergone replication-coupled incorporation of canonical H3.1/H3.2, suggests specific, active H3.3 functions distinct from maintenance of overall H3 levels.

Post-mitotic H3.3 mediates developmental acquisition of the neuronal transcriptome

The initial accumulation of H3.3 in post-mitotic neurons coincides with a critical period for the developmental establishment of the neuronal transcriptome. Indeed, recent studies have revealed that cortical neuron identity is dependent on a number of post-mitotic transcription factors (69-71, 73-75, 80-85). Co-deletion of *H3f3a* and *H3f3b* from new neurons (dKO-N) abrogates post-mitotic H3.3 accumulation and leads to widespread transcriptional changes. In particular, loss of neuronal H3.3 reduces the expression of genes that normally undergo a progressive upregulation over the course of forebrain development. Many of these genes are characterized by early (~E10.5) bivalency that is neonatally resolved to transcriptionally active chromatin. Our study indicates that H3.3 establishes the neuronal transcriptome in part by upregulating early bivalent genes and implicates a potential contribution of H3.3 to the developmental resolution of these loci. We find that in addition to decreases in gene expression, neuronal H3.3 loss also leads to significant increases, suggesting that H3.3 can contribute to the neuronal transcriptome by both activation and repression of transcription. Together, our *in vivo* analyses of dKO-N support a post-mitotic requirement for *de novo* H3.3 in establishing the neuronal transcriptome. Consistent with this possibility, *H3f3a* and *H3f3b* deletion from cycling NPCs (dKO-E) leads to remarkably similar transcriptomic changes compared to dKO-N. A minority of the transcriptional changes,

however, are unique to dKO-E, suggesting that the comparatively minor deposition of H3.3 in cycling NPCs may contribute to additional aspects of H3.3-dependent gene regulation.

Histone variants can incorporate into specific genomic regions, interact with chromatin-binding factors, and regulate nucleosome turnover (3, 5, 18-22). Deficits in these processes can contribute to the gene regulatory consequences of *H3f3a* and *H3f3b* co-deletion in dKO-N. H3.3 is preferentially incorporated into the genome at enhancers and promoters (18, 20, 28-33). It is possible that intrinsic features of H3.3-containing chromatin can influence these gene regulatory regions. However, nucleosome core particles containing canonical H3.1/H3.2 versus H3.3 have identical crystal structures (86), and at regulatory regions, nucleosome exchange is equally frequent for both H3.1 and H3.3 (32). At the protein sequence level, the H3.3S31 residue is unique to H3.3 and absent from canonical H3.1/H3.2. Phosphorylation of H3.3S31 can induce p300-dependent acetylation, particularly at enhancers (87). H3.3S31 phosphorylation is carried out by the mitotic checkpoint kinase CHEK1 (87); its potential significance in post-mitotic neurons has yet to be explored. The incorporation of H3.3 at gene regulatory regions is largely mediated by the HIRA chaperone complex (2, 5, 22). It has been hypothesized that H3.3 can locus-dependently influence chromatin function by recruiting H3.3-specific chaperones such as HIRA, which can in turn nucleate regulatory complexes on H3.3-containing chromatin (11, 87). Whether H3.3 chaperones can recruit a diversity of regulatory complexes to chromatin remains to be elucidated.

Nucleosomes fundamentally restrict access to genomic DNA. A mechanism that provides and regulates access to DNA is nucleosome turnover, which involves histone removal followed by replacement (3, 12, 88). Nucleosome turnover occurs particularly frequently in gene regulatory regions (e.g., enhancers and promoters) (20, 32, 33). A continuous exchange of histones has been proposed to transiently expose regulatory elements, thus granting DNA-binding proteins (e.g., transcription factors) access to the underlying DNA. In addition, nucleosome turnover provides a mechanism for rapid removal of histone PTMs, which may contribute to re-establishment of the chromatin landscape during cell state transitions. H3.3 plays a crucial role in nucleosome turnover. Knockdown of H3.3 genes significantly stalls nucleosome turnover in neurons and mESCs (12, 21, 22), likely by reducing the soluble (i.e. not chromatin-bound) pool of H3.3 that is required for both nucleosomal assembly and disassembly (12). In the absence of H3.3, nucleosome turnover is reduced at both active and bivalent regulatory elements (22), and previous studies have found that H3.3 plays a role in cell state transitions, particularly in establishing new identities (34, 37, 40, 87, 89). Indeed, stalled nucleosome turnover may contribute to the broad transcriptomic dysregulation we find in *H3f3a*/*H3f3b* dKO-N. Key processes that transition cycling NPCs to post-mitotic neurons occur within the critical window of H3.3 accumulation post-mitosis. Immediately after terminal division, nucleosome turnover in new neurons may contribute to erasing histone modifications associated with cycling NPCs or early bivalency. We find that neuronal *H3f3a*/*H3f3b* co-deletion reduces the expression of genes that normally transition from early bivalency to transcriptionally active chromatin over forebrain development. Consistent with frequent turnover, bivalent domains have been shown to be enriched for H3.3 in ESCs (20, 66). It is therefore possible that a reduction in nucleosome turnover can affect the resolution of bivalency in *H3f3a*/*H3f3b* dKO-N. Nucleosome turnover may also provide access to neuronal regulatory elements during the establishment of the neuronal transcriptome. Previous studies have reported that H3.3 marks both transcriptionally active (28, 30) and repressive (20, 39) chromatin, suggesting that frequent histone turnover is associated with both gene activation and repression. In *H3f3a*/*H3f3b* dKO-N, we find broad transcriptomic changes that included a large number of significantly up- and down-regulated genes. Given the importance of enhancers in spatiotemporal regulation of forebrain gene expression (90), these transcriptional disruptions may reflect widespread dysregulation of gene regulatory elements that can be a potential consequence of stalled nucleosome turnover genome-wide. Indeed, nucleosome turnover is significantly stalled following knockdown of H3.3-encoding genes (12, 21, 22). The loss of H3.3 has been hypothesized to trigger a sensing mechanism that pauses nucleosome disassembly to prevent nucleosome depletion in the absence of histones available for reassembly (21). This sensing mechanism has yet to be characterized and its potential efficiency remains unknown. It is possible that at loci with high nucleosome turnover, such as enhancers, some

histones may be evicted without replacement in the absence of H3.3. In such a scenario, nucleosome depletion at regulatory regions may also contribute to the transcriptional disruptions in dKO-N.

Post-mitotic H3.3 is required for neuronal development

The development of neuronal identity and connectivity require molecular and cellular processes that are under precise transcriptional regulation, including the establishment of cell fates at the level of NPCs (47, 67). The molecular identities of cortical neurons, however, are not entirely specified within NPCs (69-71, 73-75, 80-85). Deep-layer neurons, for example, undergo progressive refinement after neurogenesis; newly post-migratory L6 neurons transiently co-express both L5 and L6 markers, but subsequently downregulate L5 markers at late fetal ages to establish their L6-specific identity (70). The timing of this refinement coincides with the post-mitotic accumulation of H3.3. We find following post-mitotic *H3f3a* and *H3f3b* deletion (dKO-N) that deep-layer neurons aberrantly maintain abundant co-expression of L5 and L6 markers, a developmentally immature state that is normally resolved by the late fetal ages. Neuronal H3.3 is thus required for the post-mitotic refinement that establishes distinct deep-layer neuron identities. Concomitant with the layer identity phenotypes in dKO-N, we find severe defects in axon development. The neonatal dKO-N brain is characterized by agenesis of corpus callosum and misrouting of anterior commissure axons. Corticofugal tracts are able to project out of the cortex and into the internal capsule, but largely fail to innervate their targets in dorsal thalamus, tectum, or pons, consistent with disruptions of deep-layer neuronal identities. Notably, *H3f3a* and *H3f3b* deletion from NPCs (dKO-E) leads to strikingly similar phenotypes in cortical lamination and axon development compared to dKO-N. Our results therefore suggest that although NPC deletion of *H3f3a* and *H3f3b* abrogates H3.3 deposition prior to final mitosis and causes some additional changes to the transcriptome, these changes did not cause additional phenotypic consequences compared to dKO-N. Thus, the requirement for *de novo* H3.3 in critical molecular and cellular processes of neuronal development is largely post-mitotic.

Long-term H3.3 dynamics in neurons

H3f3a and *H3f3b* are ubiquitously expressed in cell types and throughout the cell cycle, and H3.3 can be deposited DNA synthesis-independently (2, 5, 11-13). In terminally post-mitotic cells such as neurons, H3.3 is thought to be the primary source of new histone H3 that maintains overall H3 levels long-term. Indeed, previous studies have shown that H3.3 ultimately fully replaces canonical H3, reaching genome-saturating levels several months after birth in the brain and other organs (15). To assess the requirement for *de novo* H3.3 after the initial post-mitotic accumulation, we use a Tg(*Rbp4-Cre*) *H3f3a* and *H3f3b* co-deletion model (dKO-R). In dKO-R, *H3f3a* and *H3f3b* are deleted from cortical L5 neurons starting at E18.5, approximately 5 days after terminal mitosis and subsequent to substantial H3.3 accumulation in the first few post-mitotic days. Importantly, dKO-R, unlike dKO-N, is not affected by peri-natal lethality, and can therefore be used to study not only the requirement for *de novo* H3.3 after initial post-mitotic accumulation, but also the long-term dynamics of H3.3 in neurons. In phenotypic analyses of P7 cortex, we find no disruption of L5 neuronal identity or axonal projections in dKO-R. The absence of molecular and cellular phenotypes in dKO-R starkly contrasts dKO-N, and suggests that H3.3 accumulation is required in the first few days after terminal mitosis, but not after this initial H3.3 increase, for multiple aspects of neuronal development.

Next, we explore the long-term dynamics of neuronal H3.3 in dKO-R. At P0, we find no change in H3.3 levels in Tg(*Rbp4-Cre*)-expressing L5 neurons. This is consistent with our result that H3.3 is substantially increased in the first days post-mitosis; *H3f3a* and *H3f3b* co-deletion after this initial accumulation does not immediately affect H3.3 levels. Over the next several months, however, H3.3 levels decrease progressively in the absence of *de novo* H3.3. By 6 months of age, dKO-R L5 neurons have largely lost H3.3 immunostaining. Together, our results support that in neurons, after initial accumulation of H3.3 in the first post-mitotic days, H3.3 is turned over more slowly, over the course of weeks and months. We next assess total H3 levels in the absence

of *de novo* H3.3. We find by pan-H3 staining that at 6 months of age, despite loss of H3.3, L5 neurons in dKO-R do not show an observable reduction in overall H3 levels or in H3 carrying post-translational modifications H3K27me3 or H3K4me3. Our results therefore support that despite loss of H3.3, H3 levels are maintained up to six months postnatally, suggesting that H3 proteins can be produced from a non-H3.3 source in terminally post-mitotic neurons in the absence of *H3f3a*/*H3f3b*. Interestingly, although canonical H3.1 and H3.2 genes have been thought to be exclusively expressed in S-phase, there is emerging evidence that under certain circumstances, canonical histone genes can be expressed as polyadenylated transcripts in post-mitotic cells (91-93). Another possibility is that other, potentially poorly-annotated, H3-like variants exist and can compensate for the loss of H3.3 (94). It is important to note that although this potential source of H3 may be able to maintain H3 levels over the long term, it is unable to compensate for the loss of initial post-mitotic H3.3 accumulation in new neurons, as evidenced by the severe transcriptomic and phenotypic consequences in dKO-N.

H3.3 and maintenance of neuronal identity

In the absence of early H3.3 accumulation post-mitosis (dKO-N), we find marked deficits in the developmental acquisition of the neuronal transcriptome. To assess the consequences of long-term H3.3 depletion on transcriptome maintenance, we use snRNA-seq to analyze dKO-R at postnatal five weeks. Remarkably, despite significant loss of H3.3, dKO-R cells formed overlapping clusters with control cells in nearly identical UMAP space. Furthermore, by pseudo-bulk analysis of L5 neurons, we find in dKO-R a remarkable normalization of genes that are differentially expressed in dKO-N. Our results suggest that although the initial accumulation of H3.3 is required for acquiring the neuronal transcriptome, once established, *de novo* H3.3 is no longer needed to maintain much of the transcriptome. This possibility is consistent with the lack of significant reductions in total H3 or H3 carrying H3K27me3 and H3K4me3 in dKO-R. It is possible that following H3.3-dependent establishment of the neuronal transcriptome, feedforward mechanisms are sufficient to enforce long-term regulation of neuronal identity genes. Together, our data support crucial H3.3 functions in the developmental acquisition, but not long-term maintenance, of neuronal identity, and we identify the first post-mitotic days as a critical window for *de novo* H3.3. Previous studies have reported a role for H3.3 in plasticity-related transcription in adult brain (21, 95). Although we find in dKO-R no changes in the developmental acquisition of much of the neuronal transcriptome, we do find a number of differentially regulated genes in dKO-R L5 PT that are associated with synaptic activity. Therefore, in mature neurons, H3.3 may function by fine-tuning transcription, an activity that is distinct from its role in establishing neuronal transcription and identity in newly post-mitotic neurons.

Materials and Methods

Experimental Animals

The *H3f3a* (JAX: 021788) and *H3f3b* (JAX: 021789) floxed alleles (52), and *Neurod6*^{Cre} (MGI:2668659) (53), *Emx1*^{Cre} (JAX: 005628) (54), Tg(*Rbp4-Cre*) (MMRRC_031125-UCD) (78, 79), and *ROSA*^{tdTomato} (JAX: 007914) (96) mice were previously generated. For timed pregnancies, the date of vaginal plug was considered embryonic day (E)0.5. Genotyping was performed using DreamTaq Green 2x Master Mix (Thermo Fisher) and genomic DNA isolated from toe or tail clips. Mice were maintained on a standard 12 h day:night cycle with *ad libitum* access to food and water, and all experiments were carried out in compliance with ethical regulations for animal research. Our study protocol was reviewed and approved by the University of Michigan Institutional Animal Care & Use Committee.

Genotyping primers:

H3f3a Mutant Reverse:	CGCGCCCTTCCAAACTAAT
H3f3a WT Reverse:	TGTTTCCTGGGTGCTTTACC
H3f3a Common Forward:	GGTGTAATTGAACAGGGAGTGG
H3f3b Mutant Reverse:	GGTAAAATCCGATAAGGATCGATAG
H3f3b WT Reverse:	CCTTGAACGTCGCTTGTCTC
H3f3b Common Forward:	TCTCCCTCACCAATCTCTGG
Cre Forward:	TCGATGCAACGAGTGATGAG
Cre Reverse:	TTCGGCTATACGTAACAGGG

Immunostaining and Imaging

Brains were isolated and fixed in 4% PFA overnight at 4°C with agitation and embedded in 4% low-melting agarose for sectioning. Brains were vibratome-sectioned at 70 µm using a Leica VT1000S or VT1200S. Free-floating sections were blocked and immunostained in blocking solution containing 5% donkey serum, 1% BSA, 0.1% glycine, 0.1% lysine, and 0.3% Triton X-100. Free-floating sections were incubated with primary antibodies overnight at 4°C followed by washing 3 × 5-min in PBS and incubated with the corresponding fluorescent secondary antibodies and DAPI in blocking solution for 1h at RT. Following secondary antibody staining, sections were mounted with VECTASHIELD Antifade Mounting Medium (Vector Laboratories). Images were acquired using either an Olympus SZX16 dissecting scope with Olympus U-HGLGPS fluorescent source and Q-Capture Pro 7 software to operate a Q-imaging Retiga 6000 camera, an Olympus Fluoview FV1000 confocal microscope with FV10-ASW software, or an Olympus Fluoview FV3000 confocal microscope with FV31S-SW software.

Primary and Secondary Antibodies

Rabbit monoclonal anti-H3.3	ABClonal	A13824
Rabbit polyclonal anti-panH3	Abcam	ab1791
Rabbit polyclonal anti-TBR1	Abcam	ab31940
Rat polyclonal anti-BCL11B	Abcam	ab18465
Rabbit polyclonal anti-LHX2	Sigma-Aldrich	ABE1402
Rat monoclonal anti-L1CAM	Sigma-Aldrich	MAB5272
Chicken polyclonal anti-GFP	Abcam	ab13970
Rabbit polyclonal anti-GFP	Invitrogen	A-11122
Rabbit polyclonal anti-BHLHE22	Sigma-Aldrich	HPA064872
Chicken polyclonal anti-RBFOX3	Sigma-Aldrich	ABN91
Mouse polyclonal anti-TLE4	Santa Cruz Biotechnology	sc-365406
Goat polyclonal anti-FOG-2	Santa Cruz Biotechnology	sc-9364
Mouse polyclonal anti-SATB2	Abcam	ab51502
Rabbit polyclonal anti-GAPDH	Santa Cruz Biotechnology	sc-25778
Rabbit polyclonal anti-Phospho KAP-1	Bethyl	A300-767A

Rabbit polyclonal anti-Cleaved Caspase 3	Cell Signaling Technology	966
Rabbit polyclonal anti-tRFP	Evrogen	AB233
Rabbit polyclonal anti-H3K27me3	Milipore	04-449
Rabbit polyclonal anti-H3K4me3	Abcam	ab8580
Goat polyclonal anti-SOX2	Santa Cruz Biotechnology	sc-17320
Donkey anti-Goat IgG (H+L), Alexa Fluor 488	Jackson ImmunoResearch Labs	805-545-180
Donkey anti-Rabbit IgG (H+L), Alexa Fluor 488	Jackson ImmunoResearch Labs	711-545-152
Donkey anti-Rat IgG (H+L), Alexa Fluor 488	Jackson ImmunoResearch Labs	712-545-150
Donkey anti-Chicken IgY (H+L), Alexa Fluor 488	Jackson ImmunoResearch Labs	703-545-155
Donkey anti-Mouse IgG (H+L), Alexa Fluor 488	Jackson ImmunoResearch Labs	715-545-150
Donkey anti-Mouse IgM, μ chain, Alexa Fluor 488	Jackson ImmunoResearch Labs	715-545-020
Donkey anti-Goat IgG (H+L), Alexa Fluor Cy3	Jackson ImmunoResearch Labs	705-165-147
Donkey anti-Rabbit IgG (H+L), Alexa Fluor Cy3	Jackson ImmunoResearch Labs	711-165-152
Donkey anti-Rat IgG (H+L), Alexa Fluor Cy3	Jackson ImmunoResearch Labs	712-165-153
Donkey anti-Chicken IgY (H+L), Alexa Fluor Cy3	Jackson ImmunoResearch Labs	703-165-155
Donkey anti-Rabbit IgG (H+L), Alexa Fluor 647	Jackson ImmunoResearch Labs	711-605-152
Donkey anti-Chicken IgY (H+L), Alexa Fluor 647	Jackson ImmunoResearch Labs	703-605-155
Donkey anti-Rat IgG (H+L), Cy5	Jackson ImmunoResearch Labs	712-175-153

EdU Birth-Dating

EdU was given by intraperitoneal injection at a concentration of 5 μg/g. For EdU staining, sections were permeabilized by incubation for 30 min in 0.5% Triton X-100 in PBS followed by 3 × 5-min washes in PBS. EdU staining solution was made fresh each time, containing 100 mM Tris, 4 mM CuSO4, and 100 mM ascorbic acid diluted in 1× PBS. The fluorescently labeled azide molecule was added last, and the staining cocktail was immediately added to sections for a 30-min incubation at room temperature (final concentrations of each fluorescent molecule: 4 mM AlexaFluor488-Azide [Click Chemistry Tools, 1275-1], 10 mM Cy3-Azide [Lumiprobe, A1330], 16 mM AlexaFluor647-Azide [Click Chemistry Tools, 1299-1]). After incubation, sections were washed 3 × 5 min in PBS. After EdU labeling, standard protocols were followed for immunostaining.

Western blotting

Mouse cortex was lysed in 1×SDS buffer, proteins were denatured 3 min at 95°C, separated on 4%–12% bis-Tris Gel (NuPAGE), transferred on nitrocellulose membranes, and blocked with 5% non-fat dry milk in Tris Buffer Saline buffer (TBS). Primary incubation was carried out in TBS plus 5% non-fat dry milk, washed 3 times and incubated with anti-rabbit or mouse peroxidase antibody (1:10,000, Cell Signaling) 1 hour in TBS, followed by washing and ECL Prime chemiluminescence revelation kit (Sigma).

RNA Isolation

Embryos were isolated and immediately submerged in ice-cold PBS. Neocortical tissue was dissected and flash-frozen in a dry ice-ethanol bath and stored at −80° until further processing. Tissue was resuspended in 0.5 mL of Trizol and homogenized using metal beads in a bullet blender. Chloroform was added to the sample, and the aqueous phase was isolated following centrifugation for 15 min at >20,000 g at 4 °C. The sample was transferred to a Zymo Research Zymo-Spin IC column and was processed following the manufacturer's protocol, including on-column DNA digestion. Pure RNA was eluted in DNase/RNase-free water and quantified using a Qubit fluorometer.

ClickSeq

RNA-seq libraries were generated by Click-Seq (60) from 600 ng of purified neocortical RNA. Ribosomal RNA was removed from total RNA using NEBNext rRNA Depletion Kit (NEB). ERCC RNA spike-in was included for library quality assessment (Thermo Fisher). SuperScript II (Invitrogen) was used for reverse transcription with

1:30 5 mM AzdNTP:dNTP and 3′ Genomic Adapter-6N RT primer (GTGACTGGAGTTCAGACGTGTGCTCTTCCGATCTNNNNNN). RNaseH treatment was used to remove RNA template and DNA was purified with DNA Clean and Concentrator Kit (Zymo Research). Azido-terminated cDNA was combined with the click adaptor oligo (/5Hexynyl/NNNNNNNNAGATCGGAAGAGCGTCGTGTAGGGAAAGAGTGTAGATCTCGGTGGTCGCCGTATCATT) and click reaction was catalyzed by addition of ascorbic acid and Cu^{2+}, with subsequent purification with DNA Clean and Concentrator Kit. Library amplification was performed using Illumina universal primer (AATGATACGGCGACCACCGAG), Illumina indexing primer (CAAGCAGAAGACGGCATACGAGATNNNNNNGTGACTGGAGTTCAGACGTGT) and the manufacturer's protocols from the 2× One Taq Hot Start Mastermix (NEB). To enrich for amplification products larger than 200 bp, PCR products were purified using Ampure XP (Beckman) magnetic beads at 1.25× ratio. Libraries were analyzed on TapeStation (Agilent) for appropriate quality and distribution and were sequenced at the University of Michigan sequencing core on the Illumina NovaSeq 6000 platform (PE 150 cycles).

Single-nucleus RNA sequencing

Cortices were isolated from embryonic and adult mice, and flash frozen in ethanol and dry ice. Nuclei were then isolated and processed for single-nuclei sequencing in accordance with 10x Genomics recommended protocols. (https://assets.ctfassets.net/an68im79xiti/2IcRfnCKj9MWM4eYZavFnc/47c6023e2987f63ec83173d62124ee7e/CG00055_Demonstrated_Protocol_Dissociation_Mouse_Neural_Tissue_Rev_C.pdf)
Resulting libraries were sequenced at the University of Michigan sequencing core on the Illumina NovaSeq 6000 platform (PE 150 cycles).

RNA sequencing data analysis

RNA-seq data were subject to quality-control check using FastQC v0.11.5 (https://www.bioinformatics.babraham.ac.uk/projects/download.html#fastqc). Adapters were trimmed using cutadapt version 1.13 (http://cutadapt.readthedocs.io/en/stable/guide.html). Processed reads were aligned to GENCODE GRCm38/mm10 reference genome with STAR (v2.5.2a) (97) and deduplicated according to UMI using UMI-tools (v0.5.3) (98). Read counts were obtained with htseq-count (v0.6.1p1) with intersection-nonempty mode (99). Differential expression was determined with edgeR (62). The *P* value was calculated with likelihood ratio tests and the adjusted *P* value for multiple tested was calculated using the Benjamini-Hochberg procedure, which controls false discovery rate (FDR). Intersectional analysis was done using ENCODE data from embryonic and P0 mouse forebrain. A logistic regression was applied to expression data from every gene, from E10.5 to P0 for each histone mark. From this data, genes were classified as "up" or "down" based on a p value of <.01 and a slope of > 2 or < -2. ChIP-seq intersection was done using deepTools2 (100) computeMatrix and computeHeatmap commands.

Single-nuclei data processing

Single nuclei RNA-seq (snRNA-seq) reads were pseudoaligned and counted using kallisto-bus tools (101) with kallisto v0.46.2 and bustools v0.40.0. The kallisto indexes used were generated from the GENCODE GRCm38.p6 reference genome and Ensembl 98 annotations with the lamanno workflow option to include introns. For the Tg(*Rbp4-Cre*) data, transgenes sequences and annotations were added to the index. Seurat v4.0.3 (42, 102) was used to filter, normalize, cluster, and analyze the data. Regularized negative binomial regression (Seurat::SCTransform) was used to normalize the E14.5 data and log normalization was used for the Tg(*Rbp4-Cre*) data. Seurat was then used to determine clusters with original Louvain algorithm and marker genes were found using a Wilcoxon Rank Sum test.

Image data analysis

Age- and section level-matched images of dKO and control mice were processed in ImageJ and Adobe Photoshop. Quantification was performed using ImageJ, Cellpose (v0.6) (103) and the Python package openCV.

Statistical analysis

Statistical analyses were performed in GraphPad Prism 8 (GraphPad Software). Values were compared using an unpaired Student's *t* test with Welch's correction, or one-way ANOVA with Tukey's post hoc test.

Acknowledgments

We thank members of the Kwan laboratory for discussions and comments on the study, critical reading of the manuscript, and scientific discussions, and colleagues in the Michigan Neuroscience Institute (MNI) and Department of Human Genetics for insightful suggestions. This work was supported by the NIH (R01 NS097525 to K.Y.K., F31 NS110206 to D.Z.D., and T32 GM007544 to O.H.F.), the Brain Research Foundation (BRFSG-2016-04 to K.Y.K.), March of Dimes Foundation (No. 5-FY15-33 to K.Y.K.), and Simons Foundation Autism Research Initiative (402213 and 324586 to K.Y.K.).

References

1. A. Groth, W. Rocha, A. Verreault, G. Almouzni, Chromatin challenges during DNA replication and repair. *Cell* **128**, 721-733 (2007).
2. S. Henikoff, M. M. Smith, Histone variants and epigenetics. *Cold Spring Harbor perspectives in biology* **7** (2015).
3. S. Venkatesh, J. L. Workman, Histone exchange, chromatin structure and the regulation of transcription. *Nat Rev Mol Cell Biol* **16**, 178-189 (2015).
4. O. J. Rando, H. Y. Chang, Genome-wide views of chromatin structure. *Annu Rev Biochem* **78**, 245-271 (2009).
5. S. J. Elsaesser, A. D. Goldberg, C. D. Allis, New functions for an old variant: no substitute for histone H3.3. *Curr Opin Genet Dev* **20**, 110-117 (2010).
6. D. A. Gallegos, U. Chan, L. F. Chen, A. E. West, Chromatin Regulation of Neuronal Maturation and Plasticity. *Trends Neurosci* **41**, 311-324 (2018).
7. J. V. Goodman, A. Bonni, Regulation of neuronal connectivity in the mammalian brain by chromatin remodeling. *Curr Opin Neurobiol* **59**, 59-68 (2019).
8. L. R. Goodwin, D. J. Picketts, The role of ISWI chromatin remodeling complexes in brain development and neurodevelopmental disorders. *Mol Cell Neurosci* **87**, 55-64 (2018).
9. R. S. Wu, W. M. Bonner, Separation of basal histone synthesis from S-phase histone synthesis in dividing cells. *Cell* **27**, 321-330 (1981).
10. R. S. Wu, S. Tsai, W. M. Bonner, Patterns of histone variant synthesis can distinguish G0 from G1 cells. *Cell* **31** (1982).
11. M. S, B. LA, The roles of histone variants in fine-tuning chromatin organization and function. *Nature reviews. Molecular cell biology* **21** (2020).
12. W. Wenderski, I. Maze, Histone turnover and chromatin accessibility: Critical mediators of neurological development, plasticity, and disease. *Bioessays* **38**, 410-419 (2016).
13. L. Shi, H. Wen, X. Shi, The Histone Variant H3.3 in Transcriptional Regulation and Human Disease. *Journal of molecular biology* **429** (2017).
14. I. Maze, K. M. Noh, A. A. Soshnev, C. D. Allis, Every amino acid matters: essential contributions of histone variants to mammalian development and disease. *Nat Rev Genet* **15**, 259-271 (2014).
15. A. Tvardovskiy, V. Schwämmle, S. J. Kempf, A. Rogowska-Wrzesinska, O. N. Jensen, Accumulation of histone variant H3.3 with age is associated with profound changes in the histone methylation landscape. *Nucleic acids research* **45** (2017).
16. M. K. Urban, A. Zweidler, Changes in nucleosomal core histone variants during chicken development and maturation. *Developmental biology* **95** (1983).
17. B. Piña, P. Suau, Changes in histones H2A and H3 variant composition in differentiating and mature rat brain cortical neurons. *Developmental biology* **123** (1987).
18. C. Jin *et al.*, H3.3/H2A.Z double variant-containing nucleosomes mark 'nucleosome-free regions' of active promoters and other regulatory regions. *Nature genetics* **41** (2009).
19. Y. Mito, J. G. Henikoff, S. Henikoff, Genome-scale profiling of histone H3.3 replacement patterns. *Nature genetics* **37** (2005).
20. A. D. Goldberg *et al.*, Distinct factors control histone variant H3.3 localization at specific genomic regions. *Cell* **140**, 678-691 (2010).
21. I. Maze *et al.*, Critical Role of Histone Turnover in Neuronal Transcription and Plasticity. *Neuron* **87**, 77-94 (2015).
22. L. A. Banaszynski *et al.*, Hira-dependent histone H3.3 deposition facilitates PRC2 recruitment at developmental loci in ES cells. *Cell* **155**, 107-120 (2013).
23. L. A. Banaszynski, C. D. Allis, P. W. Lewis, Histone variants in metazoan development. *Developmental cell* **19** (2010).
24. E. Szenker, D. Ray-Gallet, G. Almouzni, The double face of the histone variant H3.3. *Cell research* **21** (2011).
25. W. F. Marzluff, E. J. Wagner, R. J. Duronio, Metabolism and regulation of canonical histone mRNAs: life without a poly(A) tail. *Nature reviews. Genetics* **9** (2008).
26. C. Huang, B. Zhu, H3.3 turnover: a mechanism to poise chromatin for transcription, or a response to open chromatin? *Bioessays* **36**, 579-584 (2014).

27. D. Ray-Gallet, G. Almouzni, The Histone H3 Family and Its Deposition Pathways. *Adv Exp Med Biol* **1283**, 17-42 (2021).
28. P. Chen *et al.*, H3.3 actively marks enhancers and primes gene transcription via opening higher-ordered chromatin. *Genes & development* **27** (2013).
29. C. Jin, G. Felsenfeld, Nucleosome stability mediated by histone variants H3.3 and H2A.Z. *Genes Dev* **21**, 1519-1529 (2007).
30. C. M. Chow *et al.*, Variant histone H3.3 marks promoters of transcriptionally active genes during mammalian cell division. *EMBO reports* **6** (2005).
31. C. Jin, G. Felsenfeld, Distribution of histone H3.3 in hematopoietic cell lineages. *Proc Natl Acad Sci U S A* **103**, 574-579 (2006).
32. A. M. Deaton *et al.*, Enhancer regions show high histone H3.3 turnover that changes during differentiation. *Elife* **5** (2016).
33. D. C. Kraushaar *et al.*, Genome-wide incorporation dynamics reveal distinct categories of turnover for the histone variant H3.3. *Genome Biol* **14**, R121 (2013).
34. S. G. Cox *et al.*, An essential role of variant histone H3.3 for ectomesenchyme potential of the cranial neural crest. *PLoS genetics* **8** (2012).
35. C. J. Lin, M. Conti, M. Ramalho-Santos, Histone variant H3.3 maintains a decondensed chromatin state essential for mouse preimplantation development. *Development (Cambridge, England)* **140** (2013).
36. B. T. Yuen, K. M. Bush, B. L. Barrilleaux, R. Cotterman, P. S. Knoepfler, Histone H3.3 regulates dynamic chromatin states during spermatogenesis. *Development* **141**, 3483-3494 (2014).
37. J. H. Yang *et al.*, Myogenic transcriptional activation of MyoD mediated by replication-independent histone deposition. *Proceedings of the National Academy of Sciences of the United States of America* **108** (2011).
38. M. C. Tang *et al.*, Contribution of the two genes encoding histone variant h3.3 to viability and fertility in mice. *PLoS Genet* **11**, e1004964 (2015).
39. C. W. Jang, Y. Shibata, J. Starmer, D. Yee, T. Magnuson, Histone H3.3 maintains genome integrity during mammalian development. *Genes & development* **29** (2015).
40. W. Xia, J. Jiao, Histone variant H3.3 orchestrates neural stem cell differentiation in the developing brain. *Cell death and differentiation* **24** (2017).
41. W. F. Marzluff, P. Gongidi, K. R. Woods, J. Jin, L. J. Maltais, The human and mouse replication-dependent histone genes. *Genomics* **80** (2002).
42. A. Butler, P. Hoffman, P. Smibert, E. Papalexi, R. Satija, Integrating single-cell transcriptomic data across different conditions, technologies, and species. *Nat Biotechnol* **36**, 411-420 (2018).
43. T. J. Nowakowski *et al.*, Spatiotemporal gene expression trajectories reveal developmental hierarchies of the human cortex. *Science* **358**, 1318-1323 (2017).
44. H. J. Kang *et al.*, Spatio-temporal transcriptome of the human brain. *Nature* **478**, 483-489 (2011).
45. M. Buschbeck, S. B. Hake, Variants of core histones and their roles in cell fate decisions, development and cancer. *Nature Reviews Molecular Cell Biology* **18**, 299-314 (2017).
46. R. F. Hevner, R. D. Hodge, R. A. Daza, C. Englund, Transcription factors in glutamatergic neurogenesis: conserved programs in neocortex, cerebellum, and adult hippocampus. *Neurosci Res* **55**, 223-233 (2006).
47. K. Y. Kwan, N. Sestan, E. S. Anton, Transcriptional co-regulation of neuronal migration and laminar identity in the neocortex. *Development* **139**, 1535-1546 (2012).
48. J. C. Silbereis, S. Pochareddy, Y. Zhu, M. Li, N. Sestan, The Cellular and Molecular Landscapes of the Developing Human Central Nervous System. *Neuron* **89**, 248-268 (2016).
49. S. Smith, B. Stillman, Stepwise assembly of chromatin during DNA replication in vitro. *The EMBO journal* **10** (1991).
50. T. C. Miller, A. Costa, The architecture and function of the chromatin replication machinery. *Current opinion in structural biology* **47** (2017).
51. D. Brush, J. B. Dodgson, O. R. Choi, P. W. Stevens, J. D. Engel, Replacement variant histone genes contain intervening sequences. *Molecular and cellular biology* **5** (1985).
52. M. C. Tang, S. A. Jacobs, L. H. Wong, J. R. Mann, Conditional allelic replacement applied to genes encoding the histone variant H3.3 in the mouse. *Genesis (New York, N.Y. : 2000)* **51** (2013).
53. S. Goebbels *et al.*, Genetic targeting of principal neurons in neocortex and hippocampus of NEX-Cre mice. *Genesis* **44**, 611-621 (2006).
54. J. A. Gorski *et al.*, Cortical excitatory neurons and glia, but not GABAergic neurons, are produced in the Emx1-expressing lineage. *J Neurosci* **22**, 6309-6314 (2002).

55. J. M. Keil *et al.*, Symmetric neural progenitor divisions require chromatin-mediated homologous recombination DNA repair by Ino80. *Nat Commun* **11**, 3839 (2020).
56. M. Alvarez-Saavedra *et al.*, Snf2h Drives Chromatin Remodeling to Prime Upper Layer Cortical Neuron Development. *Front Mol Neurosci* **12**, 243 (2019).
57. T. C. Tuoc *et al.*, Chromatin regulation by BAF170 controls cerebral cortical size and thickness. *Dev Cell* **25**, 256-269 (2013).
58. S. B. Hake *et al.*, Expression patterns and post-translational modifications associated with mammalian histone H3 variants. *The Journal of biological chemistry* **281** (2006).
59. E. McKittrick, P. R. Gafken, K. Ahmad, S. Henikoff, Histone H3.3 is enriched in covalent modifications associated with active chromatin. *Proceedings of the National Academy of Sciences of the United States of America* **101** (2004).
60. A. Routh, S. R. Head, P. Ordoukhanian, J. E. Johnson, ClickSeq: Fragmentation-Free Next-Generation Sequencing via Click Ligation of Adaptors to Stochastically Terminated 3'-Azido cDNAs. *J Mol Biol* **427**, 2610-2616 (2015).
61. L. Shi, A. Qalieh, M. M. Lam, J. M. Keil, K. Y. Kwan, Robust elimination of genome-damaged cells safeguards against brain somatic aneuploidy following Knl1 deletion. *Nat Commun* **10**, 2588 (2019).
62. M. D. Robinson, D. J. McCarthy, G. K. Smyth, edgeR: a Bioconductor package for differential expression analysis of digital gene expression data. *Bioinformatics* **26**, 139-140 (2010).
63. E. P. Consortium, An integrated encyclopedia of DNA elements in the human genome. *Nature* **489**, 57-74 (2012).
64. B. E. Bernstein *et al.*, A bivalent chromatin structure marks key developmental genes in embryonic stem cells. *Cell* **125**, 315-326 (2006).
65. M. Sachs *et al.*, Bivalent chromatin marks developmental regulatory genes in the mouse embryonic germline in vivo. *Cell Rep* **3**, 1777-1784 (2013).
66. J. Liu, X. Wu, H. Zhang, G. P. Pfeifer, Q. Lu, Dynamics of RNA Polymerase II Pausing and Bivalent Histone H3 Methylation during Neuronal Differentiation in Brain Development. *Cell reports* **20** (2017).
67. D. P. Leone, K. Srinivasan, B. Chen, E. Alcamo, S. K. McConnell, The determination of projection neuron identity in the developing cerebral cortex. *Curr Opin Neurobiol* **18**, 28-35 (2008).
68. R. J. Mullen, C. R. Buck, A. M. Smith, NeuN, a neuronal specific nuclear protein in vertebrates. *Development (Cambridge, England)* **116** (1992).
69. P. Arlotta *et al.*, Neuronal subtype-specific genes that control corticospinal motor neuron development in vivo. *Neuron* **45**, 207-221 (2005).
70. K. Y. Kwan *et al.*, SOX5 postmitotically regulates migration, postmigratory differentiation, and projections of subplate and deep-layer neocortical neurons. *Proc Natl Acad Sci U S A* **105**, 16021-16026 (2008).
71. R. Hevner *et al.*, Tbr1 regulates differentiation of the preplate and layer 6. *Neuron* **29**, 353-366 (2001).
72. R. McEvilly, M. de Diaz, M. Schonemann, F. Hooshmand, M. Rosenfeld, Transcriptional regulation of cortical neuron migration by POU domain factors. *Science* **295**, 1528-1532 (2002).
73. B. Chen *et al.*, The Fezf2-Ctip2 genetic pathway regulates the fate choice of subcortical projection neurons in the developing cerebral cortex. *Proc Natl Acad Sci U S A* **105**, 11382-11387 (2008).
74. O. Britanova *et al.*, Satb2 is a postmitotic determinant for upper-layer neuron specification in the neocortex. *Neuron* **57**, 378-392 (2008).
75. E. Alcamo *et al.*, Satb2 regulates callosal projection neuron identity in the developing cerebral cortex. *Neuron* **57**, 364-377 (2008).
76. D. Z. Doyle *et al.*, Chromatin remodeler Arid1a regulates subplate neuron identity and wiring of cortical connectivity. *Proc Natl Acad Sci U S A* **118** (2021).
77. Z. Molnár, H. J. Luhmann, P. O. Kanold, Transient cortical circuits match spontaneous and sensory-driven activity during development. *Science* **370** (2020).
78. C. R. Gerfen, R. Paletzki, N. Heintz, GENSAT BAC cre-recombinase driver lines to study the functional organization of cerebral cortical and basal ganglia circuits. *Neuron* **80** (2013).
79. D. P. Leone *et al.*, Satb2 Regulates the Differentiation of Both Callosal and Subcerebral Projection Neurons in the Developing Cerebral Cortex. *Cereb Cortex* (2014).
80. J. Tsyporin *et al.*, Transcriptional repression by FEZF2 restricts alternative identities of cortical projection neurons. *Cell Rep* **35**, 109269 (2021).
81. W. Han *et al.*, TBR1 directly represses Fezf2 to control the laminar origin and development of the corticospinal tract. *Proc Natl Acad Sci U S A* **108**, 3041-3046 (2011).
82. T. Lai *et al.*, SOX5 Controls the Sequential Generation of Distinct Corticofugal Neuron Subtypes. *Neuron* **57**, 232-247 (2008).

83. W. L. McKenna *et al.*, Tbr1 and Fezf2 regulate alternate corticofugal neuronal identities during neocortical development. *J Neurosci* **31**, 549-564 (2011).
84. F. Bedogni *et al.*, Tbr1 regulates regional and laminar identity of postmitotic neurons in developing neocortex. *Proc Natl Acad Sci U S A* **107**, 13129-13134 (2010).
85. S. Fazel Darbandi *et al.*, Neonatal Tbr1 Dosage Controls Cortical Layer 6 Connectivity. *Neuron* **100**, 831-845.e837 (2018).
86. H. Tachiwana *et al.*, Structures of human nucleosomes containing major histone H3 variants. *Acta Crystallogr D Biol Crystallogr* **67**, 578-583 (2011).
87. S. Martire *et al.*, Phosphorylation of histone H3.3 at serine 31 promotes p300 activity and enhancer acetylation. *Nature genetics* **51** (2019).
88. S. Henikoff, Nucleosome destabilization in the epigenetic regulation of gene expression. *Nat Rev Genet* **9**, 15-26 (2008).
89. H. T. Fang *et al.*, Global H3.3 dynamic deposition defines its bimodal role in cell fate transition. *Nature communications* **9** (2018).
90. E. Markenscoff-Papadimitriou *et al.*, A Chromatin Accessibility Atlas of the Developing Human Telencephalon. *Cell* **182**, 754-769.e718 (2020).
91. S. M. Lyons *et al.*, A subset of replication-dependent histone mRNAs are expressed as polyadenylated RNAs in terminally differentiated tissues. *Nucleic Acids Res* **44**, 9190-9205 (2016).
92. I. Ryu *et al.*, HuR stabilizes a polyadenylated form of replication-dependent histone mRNAs under stress conditions. *FASEB J* **33**, 2680-2693 (2019).
93. A. R. Banday *et al.*, Replication-dependent histone genes are actively transcribed in differentiating and aging retinal neurons. *Cell cycle (Georgetown, Tex.)* **13** (2014).
94. K. Maehara *et al.*, Tissue-specific expression of histone H3 variants diversified after species separation. *Epigenetics Chromatin* **8**, 35 (2015).
95. M. E. Wimmer *et al.*, H3.3 Barcoding of Nucleus Accumbens Transcriptional Activity Identifies Novel Molecular Cascades Associated with Cocaine Self-administration in Mice. *J Neurosci* **39**, 5247-5254 (2019).
96. L. Madisen *et al.*, A robust and high-throughput Cre reporting and characterization system for the whole mouse brain. *Nat Neurosci* **13**, 133-140 (2010).
97. A. Dobin *et al.*, STAR: ultrafast universal RNA-seq aligner. *Bioinformatics* **29**, 15-21 (2013).
98. T. Smith, A. Heger, I. Sudbery, UMI-tools: modeling sequencing errors in Unique Molecular Identifiers to improve quantification accuracy. *Genome Res* **27**, 491-499 (2017).
99. S. Anders, P. T. Pyl, W. Huber, HTSeq-a Python framework to work with high-throughput sequencing data. *Bioinformatics* **31**, 166-169 (2015).
100. F. Ramírez *et al.*, deepTools2: a next generation web server for deep-sequencing data analysis. *Nucleic Acids Res* **44**, W160-165 (2016).
101. P. Melsted *et al.*, Modular, efficient and constant-memory single-cell RNA-seq preprocessing. *Nat Biotechnol* **39**, 813-818 (2021).
102. Y. Hao *et al.*, Integrated analysis of multimodal single-cell data. *Cell* **184**, 3573-3587.e3529 (2021).
103. C. Stringer, T. Wang, M. Michaelos, M. Pachitariu, Cellpose: a generalist algorithm for cellular segmentation. *Nat Methods* **18**, 100-106 (2021).

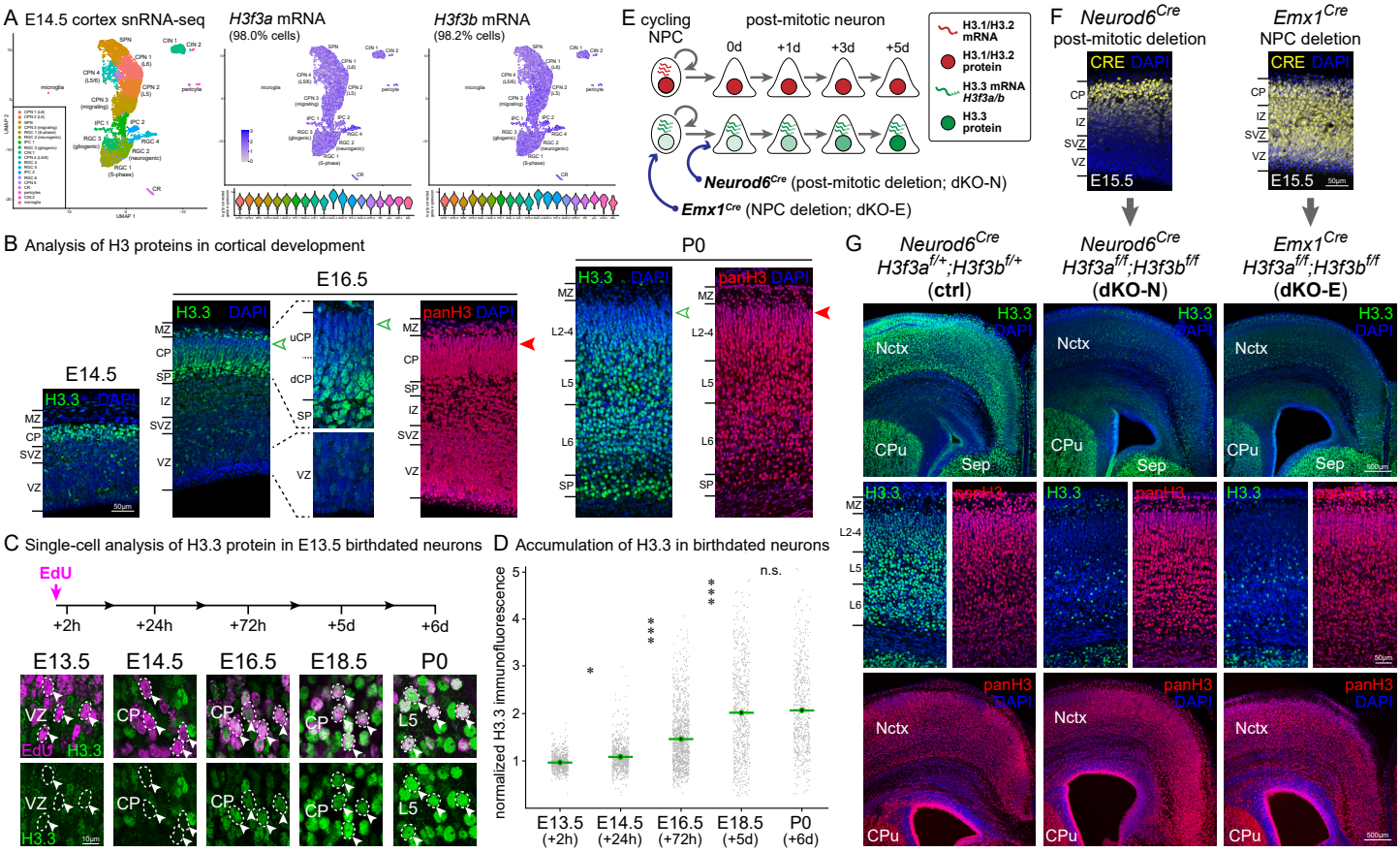

Figure 1

Post-mitotic accumulation of histone H3 variant H3.3 in cortical neurons and genetic manipulation of H3.3-encoding genes *H3f3a* and *H3f3b*. (A) Single nuclei (sn)RNA-seq of wildtype embryonic day (E)14.5 cortex visualized by Uniform Manifold Approximation and Projection (UMAP). *H3f3a* and *H3f3b* mRNA expression was found in each of the 17 identified cell clusters and in 98.0% and 98.2% of cells, respectively. (B) Analysis of variant H3.3 protein and panH3 protein in cortical development by immunostaining. On E14.5 and E16.5, low levels of H3.3 protein (green) were present in the germinal zones, ventricular zone (VZ) and subventricular zone (SVZ), composed largely of cycling neural progenitor cells (NPCs). High levels of H3.3 were present in cortical plate (CP), composed largely of post-mitotic neurons. Within the E16.5 CP and the postnatal day (P)0 cortical layers, higher levels of H3.3 were present in the early-born neurons of the subplate (SP) and deep layers, compared to the late-born neurons of the upper layers (open arrowheads). PanH3 (red) was broadly present in cortical layers and showed no preference for early-born neurons. High levels of panH3 were present in late-born upper layer neurons (solid arrowhead). (C) Temporal analysis of H3.3 accumulation. Neurons born on E13.5 were labeled by a single pulse of 5-ethynyl-2´-deoxyuridine (EdU). EdU-labeled neurons (magenta, arrowheads) were analyzed by H3.3 immunostaining (green). (D) Quantitative analysis of immunofluorescence revealed a progressive increase in H3.3 levels over the first post-mitotic days (one-way ANOVA with Tukey's post-hoc test, n.s., not significant; ∗, $p < 0.01$; ∗∗∗, $p < 0.0001$). (E) A schematic of H3.1/H3.2 and H3.3 accumulation, and genetic manipulation of H3.3-encoding genes *H3f3a* and *H3f3b*. (F) Analysis of CRE expression (yellow) by immunostaining confirmed the published specificities of *Neurod6*^{Cre} in newly post-mitotic neurons and of *Emx1*^{Cre} in NPCs. (G) Analysis of H3 proteins in P0 control (ctrl) and conditional H3.3 genes double knockouts, *Neurod6*^{Cre};*H3f3a*$^{f/f}$;*H3f3b*$^{f/f}$ (dKO-N) and *Emx1*^{Cre};*H3f3a*$^{f/f}$;*H3f3b*$^{f/f}$ (dKO-E). In both dKO-N and dKO-E, H3.3 (green) was largely lost from neocortex (Nctx) but preserved in caudate putamen (CPu) and septum (Sep). The levels of panH3 (red) were unaffected in dKO-N or dKO-E.

CPN, cortical plate neuron; SPN, subplate neuron; RGC, radial glial cell; IPC, intermediate progenitor cell; CIN, cortical interneuron; CR, Cajal-Retzius cell; MZ, marginal zone; CP, cortical plate; uCP, upper cortical plate; dCP, deep cortical plate; VZ, ventricular zone; SVZ, subventricular zone; IZ, intermediate zone; L*n*, layer *n*; NPC, neural progenitor cell; Nctx, neocortex; CPu, caudate putamen; Sep, septum

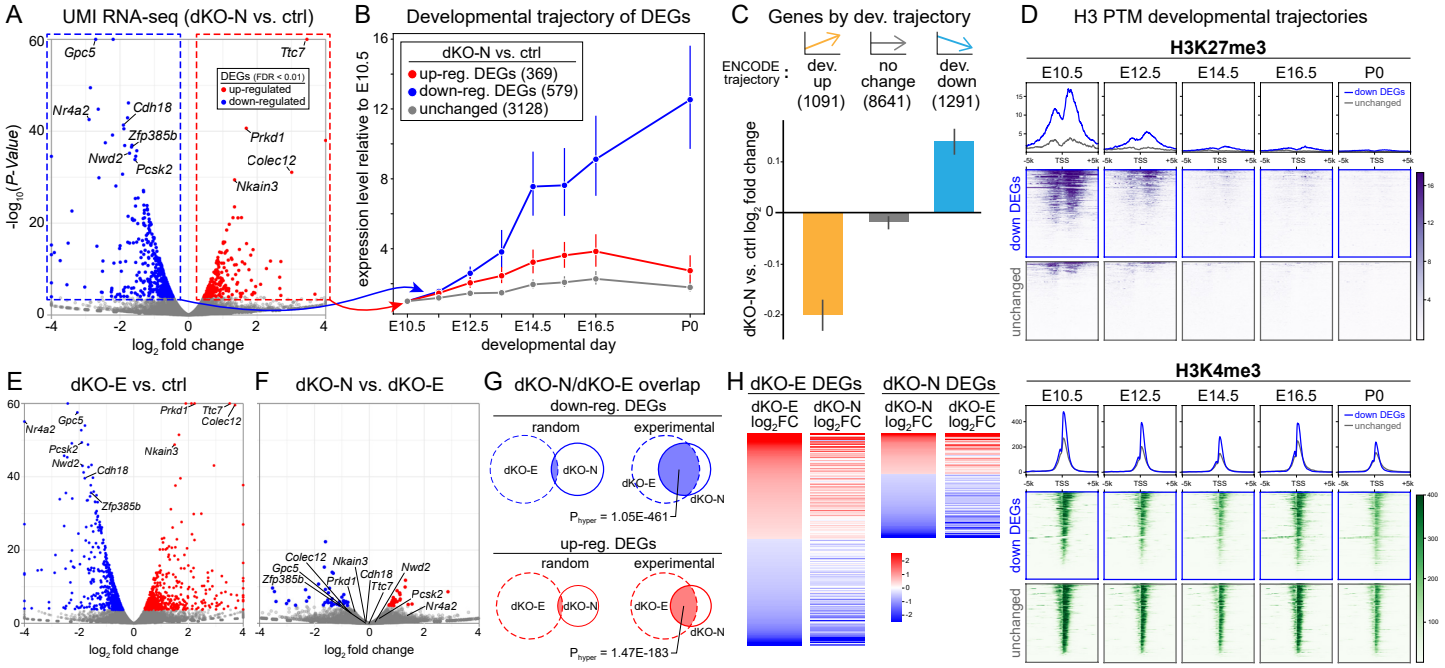

Figure 2

Disrupted developmental acquisition of the neuronal transcriptome following *H3f3a* and *H3f3b* co-deletion. (A) Volcano plot of UMI RNA-seq comparing P0 cortex of dKO-N to control. For each gene, *P* value was calculated with likelihood ratio tests and false discovery rate (FDR) was calculated using the Benjamini-Hochberg procedure. Of 948 differentially expressed genes (DEGs, FDR < 0.01), 579 were significantly down-regulated (blue dots) and 369 were significantly up-regulated (red dots). (B) The developmental expression trajectories of dKO-N DEGs and 3128 unchanged genes (FDR > 0.9, -0.1 < log_2FC < 0.1, log_2CPM > 1) based on ENCODE RNA-seq data of wildtype mouse forebrain. Expression trajectories were normalized to E10.5 levels. Genes downregulated in dKO-N were characterized by a progressive increase in expression across embryonic forebrain development. (C) Genes were categorized based on developmental trajectory using logistic regression on the ENCODE wildtype forebrain RNA-seq data. Genes that normally increase in expression over the course of embryonic development (dev. up, slope > 2, pval < 0.01) were significantly downregulated in dKO-N. (D) The developmental H3 post-translational modification (PTM) trajectories of dKO-N downregulated and unchanged genes based on ENCODE mouse forebrain ChIP-seq data. Genes downregulated in dKO-N (blue traces) are normally characterized by a progressive decrease in H3K27me3 enrichment (indigo), but not in H3K4me3 enrichment (dark green), across forebrain development. (E and F) Volcano plots comparing P0 cortex of dKO-E to control (E) and dKO-N to dKO-E (F). DEGs are indicated as in A. (G) Experimental overlap of dKO-N and dKO-E DEGs compared to random overlap based on hypergeometric probability. (H) Heatmap of dKO-N and dKO-E DEGs based on log_2FC. dKO-N and dKO-E DEGs showed highly congruent expression change directionality.

DEG, differentially expressed gene; reg., regulated; FDR, false discovery rate; dev., developmental; FC, fold change; CPM, counts per million

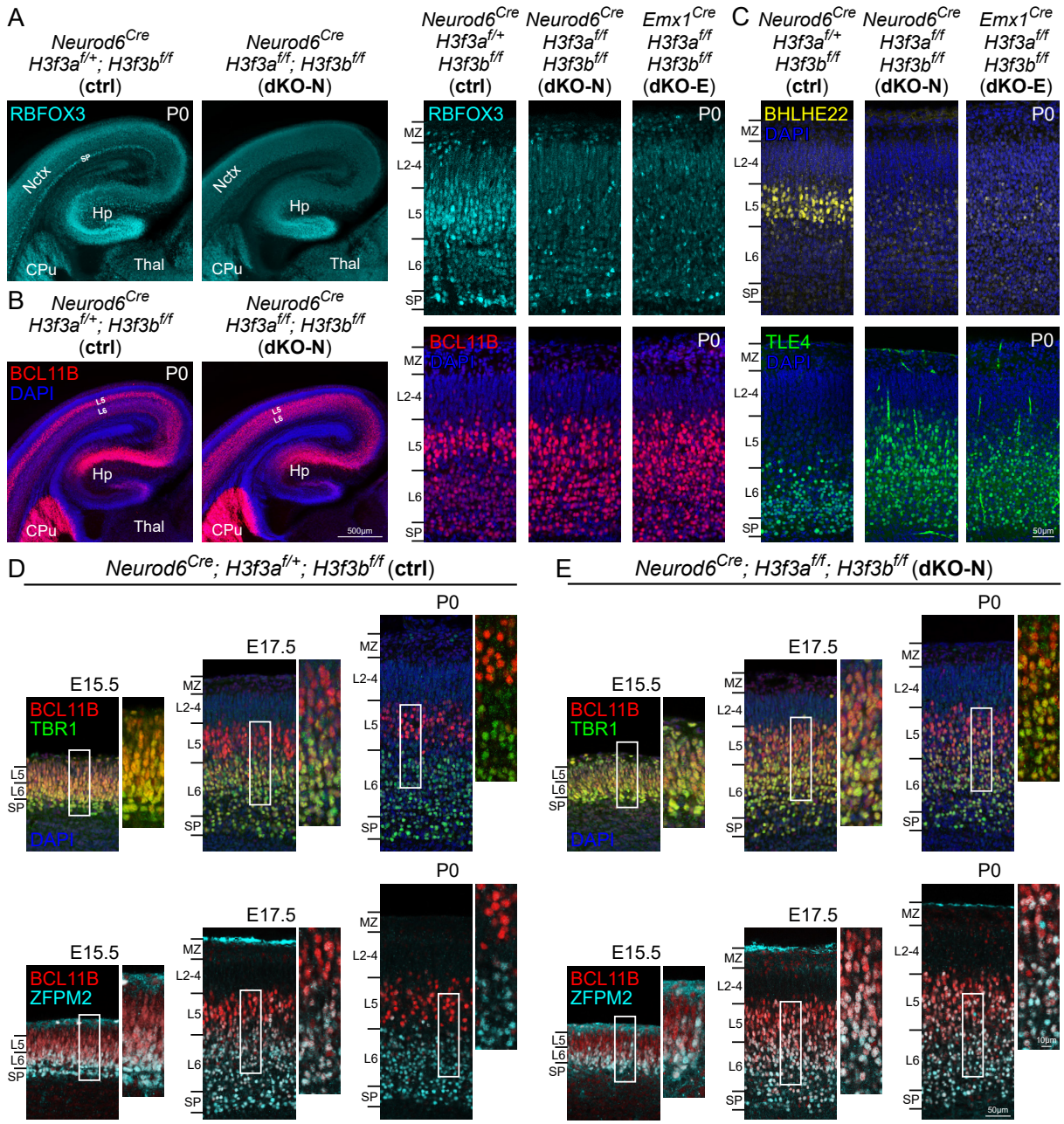

Figure 3

Disrupted establishment of layer-dependent neuronal identities following *H3f3a* and *H3f3b* co-deletion. (A) In P0 control cortex, RBFOX3 (NEUN, cyan) immunostaining was present in all cortical layers and intensely labeled L5 and SP neurons. In dKO-N and dKO-E cortex, RBFOX3 expression was decreased compared to control and intense staining of L5 and SP neurons was absent. (B) In P0 ctrl, BCL11B (CTIP2, red) showed intense staining in L5 neurons and moderate staining in L6 neurons in a stereotyped pattern. In dKO-N and dKO-E, the differential BCL11B staining between L5 and L6 was lost. (C) In P0 ctrl, BHLHE22 (yellow) immunostaining intensely labeled L5 neurons, and TLE4 (green) immunostaining was restricted to L6 neurons. In dKO-N and dKO-E, intense L5 staining of BHLHE22 was lost, and TLE4 staining was aberrantly present in L5. (D and E) Post-mitotic refinement of deep-layer neuronal identities was analyzed in E15.5, E17.5, and P0 cortex by layer marker co-staining. In control (D), TBR1 (green)- or ZFPM2 (FOG2, cyan)-labeled L6 neurons abundantly co-expressed BCL11B (red) at E15.5. TBR1- or ZFPM2-labeled L6 neurons have begun to downregulate BCL11B at E17.5 and largely did not express high levels of BCL11B by P0. In dKO-N (E), BCL11B was co-expressed with TBR1 or ZFPM2 at E15.5 in a manner similar to control. Abundant marker co-expression, however, persisted at E17.5 and P0. Deep-layer neurons maintained a developmentally immature, mixed L5/L6 molecular identity in dKO-N until P0.

Hp, hippocampus; Thal, thalamus

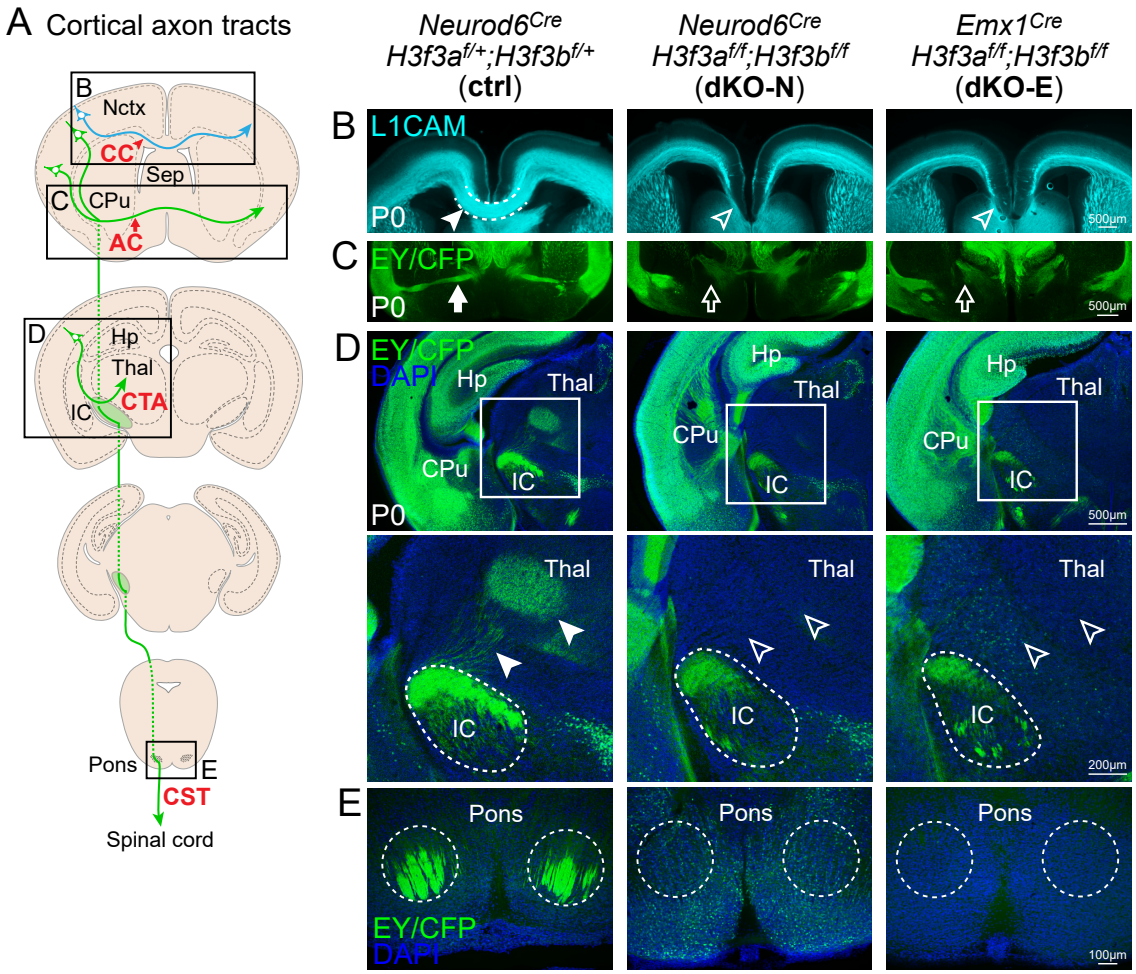

Figure 4

Defective axon tract development following *H3f3a* and *H3f3b* co-deletion. (A) A schematic of major cortical axon tracts. (B) L1CAM (cyan) staining of P0 ctrl, dKO-N, and dKO-E cortex. dKO-N and dKO-E were characterized by a loss of white matter thickness and complete agenesis of corpus callosum (CC, arrowheads). (C-E) Cre-dependent fluorescent reporters expressed from the *H3f3a* and *H3f3b* floxed loci were detected by EGFP immunostaining of EYFP and ECFP residues and used to analyze axon tracts in P0 ctrl, dKO-N, and dKO-E cortex. (C) EY/CFP (green) reporter staining revealed failed midline crossing of the anterior commissure (AC, arrows) and misrouting of anterior commissure axons to the hypothalamus in dKO-N and dKO-E. (D) In dKO-N and dKO-E, corticofugal axons reached the internal capsule (IC), but the corticothalamic tract (CTA, arrowheads) did not form. (E) Analysis of the corticospinal tract (CST) revealed an absence of axons that reached the level of the pons in dKO-N and dKO-E.

CC, corpus callosum; AC, anterior commissure; CTA, corticothalamic tract; CST, corticospinal tract; IC, internal capsule

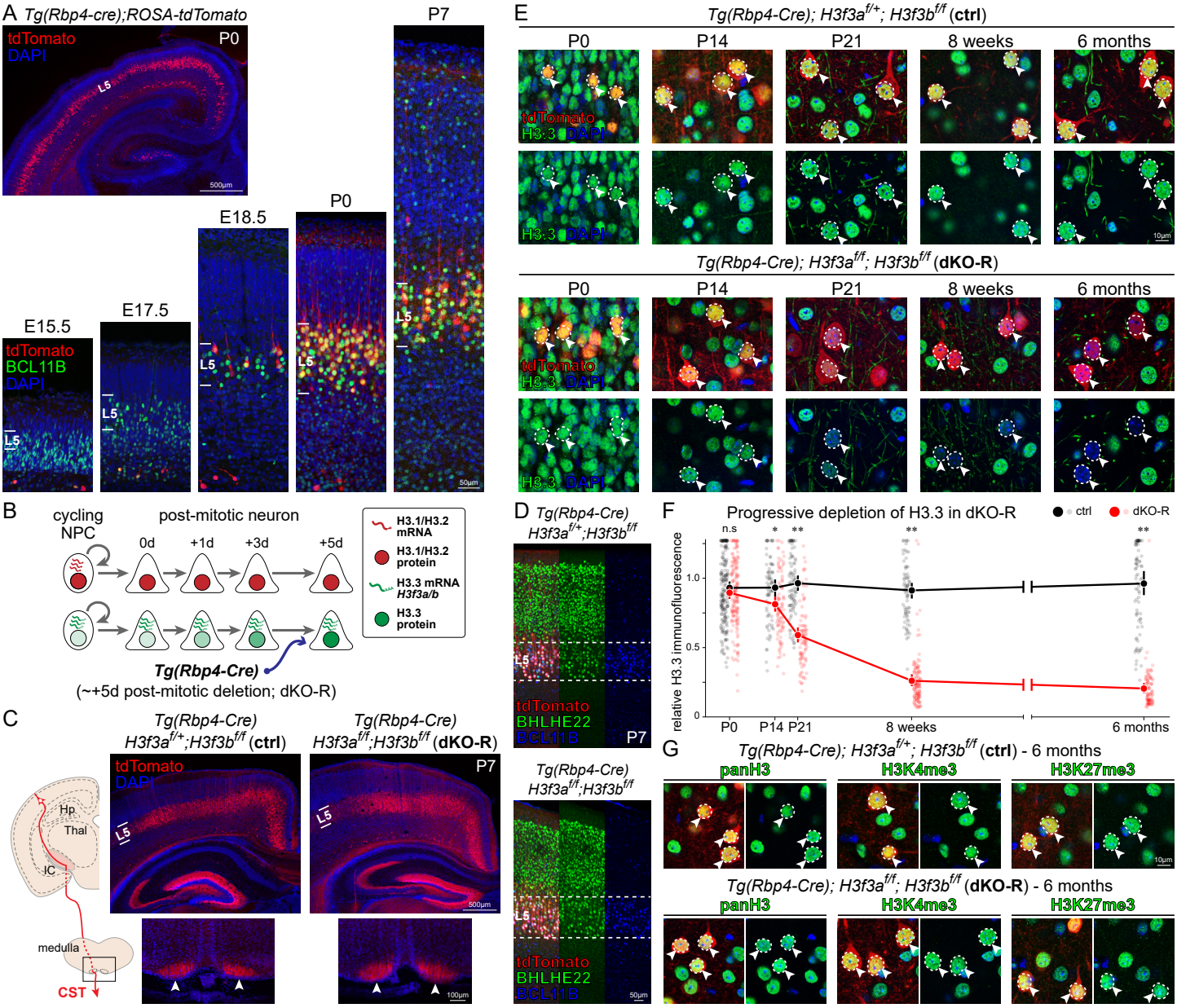

Figure 5

H3f3a and *H3f3b* co-deletion after initial H3.3 accumulation in new neurons. (A) Spatiotemporal analysis of Tg(*Rbp4-Cre*)-mediated recombination by Cre-dependent reporter *ROSA-tdTomato* (red) across cortical development. Tg(*Rbp4-Cre*)-mediated recombination was present in BCL11B-labeled (green) L5 neurons starting at ~E18.5, approximately 5 days after terminal mitosis. (B) A schematic of H3.3 accumulation and genetic manipulation of *H3f3a* and *H3f3b* by Tg(*Rbp4-Cre*): Tg(*Rbp4-Cre*);*H3f3a*$^{f/f}$;*H3f3b*$^{f/f}$ (dKO-R). (C) At P7, tdTomato-labeled axons (red) arising from L5 neurons abundantly innervated the corticospinal tract (CST) and reached the pyramids (arrowheads) at the level of the medulla in dKO-R in a manner indistinguishable from control. (D) Analysis of BHLHE22 (green) and BCL11B (blue) by immunostaining revealed normal BHLHE22/BCL11B co-expression in tdTomato-labeled L5 neurons (red) in dKO-R. (E) Temporal analysis of H3.3 levels in tdTomato-labeled L5 neurons (red, arrowheads) by immunostaining. In control cortex, H3.3 (green) is maintained in tdTomato-labeled L5 neurons at each analyzed age. In dKO-R, H3.3 levels were unaffected at P0 but showed a progressive loss from L5 neurons over weeks and months. (F) Quantitative analysis of immunofluorescence (unpaired t-test with Welch's correction, n.s., not significant; ✻, $p < 0.01$; ✻✻, $p < 0.001$). (G) At postnatal 6 months, panH3 and H3 carrying post-translational modifications (PTMs) H3K4me3 and H3K27me3 (green) were assessed by immunostaining. In tdTomato-labeled L5 neurons (red, arrowheads) in dKO-R, despite loss of H3.3 at this age, the levels of panH3 and H3 carrying PTMs were not observably different compared to control.

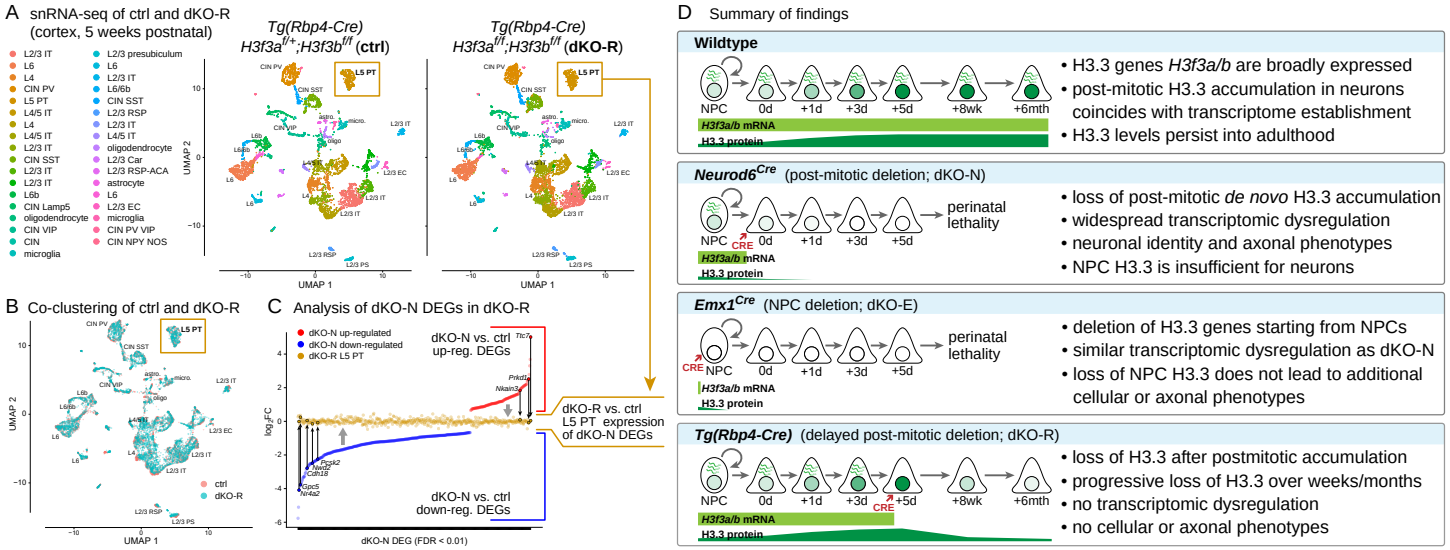

Figure 6

Maintenance of neuronal transcriptome following *H3f3a* and *H3f3b* co-deletion after initial H3.3 accumulation. (A and B) snRNA-seq of control and dKO-R cortex at postnatal 5 weeks visualized by UMAP. Clustering of ctrl and dKO-R cells showed the same 34 cell clusters in UMAP space (A) with substantial overlap of each cluster (B), including the L5 pyramidal tract (PT) neurons (gold boxes) in which Tg(*Rbp4-Cre*) is active. (C) Differentially expressed genes (DEGs) from dKO-N were compared based on $\log_2$FC in dKO-N and in dKO-R L5 PT. Both up- and down-regulated dKO-N DEGs showed a normalization towards a $\log_2$FC of 0 (no change) in dKO-R L5 PT (arrows). (D) Summary of key findings. Cortical neurons undergo substantial *de novo* H3.3 accumulation post-mitosis. *De novo* H3.3 in post-mitotic neurons is required for developmental acquisition of the neuronal transcriptome, establishment of distinct neuronal identities, and formation of axon tracts. The first few post-mitotic days are a critical window for *de novo* H3.3 in neurons. This early H3.3 accumulation differs in timescale from long-term H3.3 turnover, which occurs over weeks to months in cortical neurons.